INFORMATION TO USERS

This reproduction was made from a copy of a document sent to us for microfilming. While the most advanced technology has been used to photograph and reproduce this document, the quality of the reproduction is heavily dependent upon the quality of the material submitted.

The following explanation of techniques is provided to help clarify markings or notations which may appear on this reproduction.

1. The sign or "target" for pages apparently lacking from the document photographed is "Missing Page(s)". If it was possible to obtain the missing page(s) or section, they are spliced into the film along with adjacent pages. This may have necessitated cutting through an image and duplicating adjacent pages to assure complete continuity.

2. When an image on the film is obliterated with a round black mark, it is an indication of either blurred copy because of movement during exposure, duplicate copy, or copyrighted materials that should not have been filmed. For blurred pages, a good image of the page can be found in the adjacent frame. If copyrighted materials were deleted, a target note will appear listing the pages in the adjacent frame.

3. When a map, drawing or chart, etc., is part of the material being photographed, a definite method of "sectioning" the material has been followed. It is customary to begin filming at the upper left hand corner of a large sheet and to continue from left to right in equal sections with small overlaps. If necessary, sectioning is continued again—beginning below the first row and continuing on until complete.

4. For illustrations that cannot be satisfactorily reproduced by xerographic means, photographic prints can be purchased at additional cost and inserted into your xerographic copy. These prints are available upon request from the Dissertations Customer Services Department.

5. Some pages in any document may have indistinct print. In all cases the best available copy has been filmed.

University Microfilms International
300 N. Zeeb Road
Ann Arbor, MI 48106

FRIEDLANDER, MICHAEL ARTHUR

AN EXPERIMENTAL ANALYSIS OF THE FISSILE CONTENT OF THE TRIGA CORE BY TRANSFER FUNCTION MEASUREMENT

THE UNIVERSITY OF ARIZONA M.S. 1984

AN EXPERIMENTAL ANALYSIS OF THE FISSILE CONTENT OF THE TRIGA CORE BY TRANSFER FUNCTION MEASUREMENT

by

Michael Arthur Friedlander

A Thesis Submitted to the Faculty of the

DEPARTMENT OF NUCLEAR AND ENERGY ENGINEERING

In Partial Fulfillment of the Requirements
For the Degree of

MASTER OF SCIENCE

In the Graduate College

THE UNIVERSITY OF ARIZONA

1 9 8 4

STATEMENT BY AUTHOR

This thesis has been submitted in partial fulfillment of requirements for an advanced degree at The University of Arizona and is deposited in the University Library to be made available to borrowers under the rules of the Library.

Brief quotations from this thesis are allowable without special permission, provided that accurate acknowledgement of source is made. Request for permission for extended quotation from or reproduction of this manuscript in whole or in part may be granted by the head of the major department or the Dean of the Graduate College when in his judgment the proposed use of the material is in the interests of scholarship. In all other instances, however, permission must be obtained from the author.

SIGNED: Michael C. Snodgrass

APPROVAL BY THESIS DIRECTOR

This thesis has been approved on the date shown below:

Barry Ganapol — May 25, 1984

B. GANAPOL — Date

Professor of Nuclear Engineering

ACKNOWLEDGMENTS

The author wishes to express his gratitude to the faculty and staff of the Department of Nuclear and Energy Engineering and in particular to Dr. Barry Ganapol, Dr. David Hetrick, and to Dr. George Nelson. Thanks goes to Mr. Harry Doane, Mr. Dan Beeson and to Mr. Nathan Moyer for their mechanical and electronic expertise. He is also deeply grateful to Los Alamos National Laboratory for the guidance and opportunities he received, especially from Dr. George Eccleston. A special thanks goes to his family and friends for their emotional support and to his wife, Cheryl, for her encouragement and sacrifice.

TABLE OF CONTENTS

LIST OF ILLUSTRATIONS

LIST OF TABLES

ABSTRACT

Several alternative methods for measuring the fissile content of reactor fuel were investigated. The methods analyzed involved making dynamic measurements of the reactor transfer function and correlating the measurements with known or assumed fundamental reactor parameters. Dynamic measurements of the neutron population in a multiplying assembly can give qualitative and quantitative information about local neutronic characteristics and identify different fissile isotopes and elements in a non-destructive manner.

Two different devices were built and tested, and a third system was investigated. The experiments included evaluating the plutonium and uranium content of standard TRIGA fuel elements and the University of Arizona Research Reactor and determining the U-235 content of a standard 15X15 fresh PWR fuel assembly. Although the results are inconclusive, the theory and measurements agree well enough to warrant further investigation.

CHAPTER 1

INTRODUCTION

With the initiation of the Manhattan Project in the early 1940's, came the need for non-destructive assay (NDA) techniques for quantitative measurements of fissile and fertile materials. However, because of the relatively small scale use and the highly controlled access, the safeguards concepts of today were unknown. Accountability measures were necessary for criticality safety, so methods were developed to measure characteristic radiations eminating from samples of radioactive materials, in particular fissile isotopes.

During the mid 1960's, the expansion of the private nuclear industry coupled with the institution of the Nuclear Non-Proliferation Treaty, made widespread use of non-destructive assay necessary. Non-destructive assay was required to detect and prevent theft and diversion of Special Nuclear Material (SNM). In response to this need, a host of methods and techniques were developed. In 1966, Los Alamos National Laboratory (LASL) developed a method of interrogating samples with 14 MeV neutrons (Gozani, 1981). In 1967, Gulf General Atomic developed a method of interrogation using high energy gamma rays. Monsanto Research

Laboratory developed a calorimetric method of plutonium assay. The Helix-Counter was developed to measure plutonium at Rocky Flats, and Brookhaven National Laboratory developed the neutron well counter for plutonium assay.

In the previous list of developments two methods of assay are presented: active and passive NDA. Each method has its own characteristics, advantages, and disadvantages. The Active NDA (ANDA) approach is followed at LASL, that is, using a source of neutrons to excite the sample and measure the effect. This technique allows precise measurement of small samples of special nuclear material, but immobility of neutron sources limit its application. Passive NDA (PNDA) measures the internal release of neutrons by spontaneous fission of isotopes. A device utilizing this technique relieves the requiremement of having a neutron source, however, it is accurate only for large quantities of materials that spontaneously emit neutrons. Because of the drawbacks associated with traditional ANDA and PNDA techniques, a method was sought that combined the advantageous properties of conventional methods and minimized the disadvantages.

The purpose of the investigation to be presented is to determine the feasibility of an ANDA-PNDA hybrid for safeguards use. The hybrid consists of a mechanism designed

to cause the reactivity of The University of Arizona TRIGA Research Reactor to fluctuate in a sinusoidal manner. A series of dynamic measurements of the neutron population in the core will be made and correlated with the reactivity oscillation. From this information, a value for the fractions of fissile isotopes contributing to the neutron population can be made as well as determining some of the neutronic characteristics in the vicinity of the reactivity oscillator. Theoretical considerations will be given as well as the results of an experiment utilizing the technique. Also, a brief presentation of some preliminary investigations will be given.

CHAPTER 2

TRANSFER FUNCTIONS

The basic premise of non-destructive assay is to derive information about the system in a non-evasive manner. As mentioned, several methods are available for doing this, however, all involve perturbing the system in some manner and looking at the results. In general systems, the results can be predicted numerically and characterized by a parameter known as the transfer function.

Black Box Transfer Functions

Assume that in Figure 1, x(t) is an input to a "BLACK BOX" which acts on it in a manner H, and outputs a signal y(t), varying in time. Take the Laplace Transform of the input, the output and the operator H. If the system in Figure 1 is linear, the relationship between the three variables is,

$$Y(s) = H(s)\ X\ (s) \qquad 2.1.1$$

where

$$Y(s) = \int_0^\infty dt\ e^{-st} y(t) \qquad 2.1.2$$

$$X(s) = \int_0^\infty dt\ e^{-st}\ x(t) \qquad 2.1.3$$

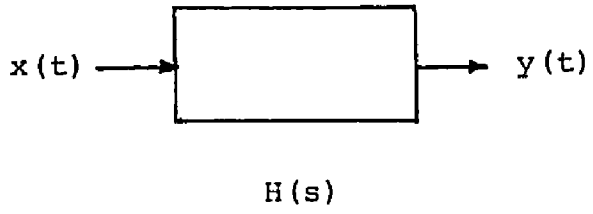

Figure 1. Black Box

And upon rearranging,

$$H(s) = \frac{Y(s)}{X(s)} \qquad 2.1.4$$

From equation 2.1.4, information about the "BLACK BOX" can be derived by observing the ratio of the transform of the output to the transform of the input. The ratio in equation 2.1.4 is defined as the transfer function.

To determine the significance of the transfer function, take the inverse transform of equation 2.1.1. This is

$$y(t) = \frac{1}{2\pi i}\int_{\gamma-i\infty}^{\gamma+i\infty} ds\, e^{st} H(s)X(s) \qquad 2.1.5$$

The magnitude of the transfer function, also known as the gain is

$$\left|H(s)\right|^2 = (\text{Re } H(S))^2 + (\text{Im } H(s))^2 \qquad 2.1.6$$

and the phase of the transfer function is

$$\phi = \tan^{-1} \frac{\text{Im } H(s)}{\text{Re } H(s)} \qquad 2.1.7$$

Reactor Transfer Function

In a neutron multiplying assembly, the point reactor kinetics equations,

$$\frac{dn}{dt} = \frac{\rho-\beta}{\ell} n + \sum_{i=1}^{6} \lambda i\, Ci + q_o \qquad 2.2.1$$

$$\frac{dci}{dt} = \frac{\beta i}{\ell} n - \lambda i ci \qquad 2.2.2$$

Where n is the neutron population in neutrons,

ℓ is the neutron generation time, in seconds,

β_i is the fraction of neutrons emitted by the decay of the i^{th} group of the delayed neutron precursors.

λ_i is the decay constant of the ith group of delayed neutron precursors, in seconds -1,

q_o is the source strength, in neutrons/second,

ρ is the reactivity, (k-1)/k

characterize the time-dependent neutron population in a multiplying assembly. If the reactivity is a function of the neutron population, equations 2.2.1 and 2.2.2 become non-linear, coupled differential equations. Assume the reactivity, delayed neutron precursor concentration, source strength and neutron population can be linearized in the following form,

$$\rho = \rho_o + \delta\rho \qquad 2.2.3$$

$$ci = ci + \delta ci \qquad 2.2.4$$

$$q = q_o \qquad 2.2.5$$

$$n = n_o + \delta n \qquad 2.2.6$$

where a δ indicates a small change about the steady state value. Furthermore, in the steady state, all time derivatives vanish and it can be shown that the steady state precurson concentration and source strength are given by

$$ci_o = \frac{\beta i \quad n_o}{\ell \quad \lambda i} \qquad 2.2.7$$

$$q = - \frac{\rho_o n_o}{\ell} \qquad 2.2.8$$

Substituting equations 2.2.3, 2.2.4, 2.2.5, 2.2.6, 2.2.7, and 2.2.8 into equations 2.2.1 and 2.2.2 and neglecting terms of order δ^2 gives

$$\frac{d}{dt} \quad (\delta n) = \frac{\rho_o \beta}{\ell} \quad \delta n \quad + \quad \sum_{i=1}^{6} \quad \lambda i \ \delta ci + \frac{n_o}{\ell} \qquad 2.2.9$$

$$\frac{d}{dt} \quad (\delta ci) = \frac{\beta i}{\ell} \quad \delta n - \lambda i \ \delta ci \qquad 2.2.10$$

Taking the Laplace Transform of equations 2.2.9 and 2.2.10, and solving the transform of δn gives

$$N(s) = \frac{\delta n(_o) + \sum_{i=1}^{6} \frac{\lambda i \ \delta ci(_o)}{s + \lambda i} + \frac{N_o}{\ell} R(s)}{s + \frac{\beta - \rho_o}{\ell} - \frac{1}{\ell} \sum_{i=1}^{6} \frac{\beta i \ \lambda i}{s + \lambda i}} \qquad 2.2.11$$

where

N(s) is the Laplace Transform of n

R(s) is the Laplace Transform of p

Taking the Inverse Laplace Transform of equation 2.2.11 gives many terms, all but one of which will decay in time. The transform of the remaining term is given by

$$N(s) = \frac{n_o \ R(s)}{s\ell + \beta - \rho_o \sum_{i=1}^{6} \frac{\beta i \ \lambda i}{s + \lambda i}} \qquad 2.2.12$$

Now postulate that

$$\delta\rho = c_1 \sin \omega t \qquad 2.2.13$$

The Laplace Transform of equation 2.2.13 is

$$R(s) = \frac{c_1 \omega}{s^2 + \omega^2} \qquad 2.2.14$$

Substituting equation 2.2.14 into equation 2.2.12 gives

$$N(s) = \frac{\dfrac{c_1 \omega n_o}{s^2 + \omega^2}}{s\ell + \beta - \rho_o - \sum_{i=1}^{6} \dfrac{\beta i \lambda i}{s + \lambda i}} \qquad 2.2.15$$

If the reactivity of the system is negative, the roots of the denominator of equation 2.2.15 are in the left half plane. The inverse Laplace transform of equation 2.2.15 can be found from the sum of the residues at the two poles of the numerator, namely $\pm i\omega$. The residue of equation 2.2.15 at $\pm i\omega$ is given by

$$\text{Res}\ (N\ (i\ \omega)) = \lim_{s \to i\omega} \frac{(s - i\omega)\ \dfrac{c_1 \omega n_o e^{st}}{s^2 + \omega^2}}{s\ell + \beta - \rho_o - \sum_{i=1}^{6} \dfrac{\beta i \lambda i}{s + \lambda i}}$$

$$\text{Res}\ (N\ (-i\omega)) = \lim_{s \to i\omega} \frac{(s - i)\ \dfrac{c_1 \omega n_o e^{st}}{s^2 + \omega^2}}{s\ell + \beta - \rho_o - \sum_{i=1}^{6} \dfrac{\beta i \lambda i}{s + \lambda i}} \qquad 2.2.16$$

$$2.2.17$$

Assume that $N(i\omega)=N(i\omega)$. Evaluating the sum of the residues gives an expression for the sustained neutron population as a function of time,

$$n(t) = c_1 n_o \left| G\ (i\omega) \right| \sin(\omega t+\phi) \qquad 2.2.18$$

where $G(i\omega)$ is the Reactor Transfer Function and is given by

$$G(i\omega) = \frac{1}{i\omega \ell+\beta - \rho_o - \sum_{i=1}^{6} \frac{\beta i\ \lambda i}{i\omega +\lambda i}} \qquad 2.2.19$$

$$\phi = \tan^{-1} \frac{-\omega \ell+ \sum_{i=1}^{6} \frac{\beta i\ \lambda i}{w^2 + \lambda i^2}}{\beta- \rho_o - \sum_{i=1}^{6} \frac{\lambda^2 i\ \beta i}{\lambda i^2 +w^2}} \qquad 2.2.20$$

The physical significance of the phase and gain of the transfer function can be seen in equation 2.2.18. The gain is the measure of how far above the steady state the neutron population swings, that is, it is a measure of the amplitude of the power swing. The phase of the transfer function gives a measure of how far the power lags behind the reactivity oscillation. Both numbers can be used to determine basic reactor parameters.

The assumptions mentioned pose some restrictions. Assuming that the equations can be linearized means that the deviations from steady state must be small. Assuming

that $N(i\omega)=N(-i\omega)$ is equivalent to assuming that the result of the inversion is real. It was assumed that the reactivity of the system was negative, that is, the roots of the denominator of equation 2.2.15 are in the left half plane. If this is not true, equation 2.2.18 is still valid, however, the sine wave is superimposed on a growing exponential.

CHAPTER 3

NUMERICAL METHODS OF ANALYZING DATA

One of the most commonly measured parameters of data is the time dependent or dynamic response. The reasons for this are two-fold. First, time dependence is easily measured. Multichannel analyzers exist to record data in time increments on the order of microseconds, thereby allowing high precision measurements. Secondly, the dynamic response yields information about the inside of the system, without opening it up. This is useful because it allows measurements of parameters of systems that would otherwise be unextractable, either because of safety reasons or because of the nature of the parameter, such as the fundamental quality β/ℓ in a nuclear reactor. Also, it is not necessary to destroy the system being measured.

One technique of analyzing data is by cross-correlation. Analytically expressed, the cross correlation of an excitation function, x(t) and the output function, y(t) is given by

$$\phi_{xy} = \frac{1}{T} \int_{o}^{T} dt\,(x(t)-\bar{x})\,(y(t+\tau) - \bar{y}) \qquad 3.1.1$$

where x(t) is the excitation function

y(t) is the output function

T is the period over which x(t) and y(t) are defined

τ is a time lag or lead

$\bar{x}$ is the average x given by

$$\bar{x} = \frac{1}{T}\int_{o}^{T} dt\ x(t) \qquad 3.1.2$$

$\bar{y}$ is the average y given by

$$\bar{y} = \frac{1}{T}\int_{o}^{T} dt\ y(t) \qquad 3.1.3$$

The virtue of performing such a computation is that noise in the signal does not strongly affect the result of the integration. Therefore, useful data can be extracted in the situation where a relatively small signal to noise ratio exists. This type of measurement can be carried out by, (a) exciting a system with a known function, and then, (b) by measuring the output, compute the integral in equation 3.1.1

While equation 3.1.1 is an exact expression, analytical expressions for x(t) and y(t) are rarely realized. Instead, digital data usually exists as a function of time. Also, a normalization is often used, where $\phi xy=1$ implies that x and y are perfectly correlated, and $\phi xy=0$ implies that x and y are completely uncorrelated. Approximating equation 3.1.1 by a finite number of data points and applying the normalization gives

$$\phi_{xy} = \frac{\frac{1}{N}\sum_{K=1}^{N} (x(K)-\bar{x})\ (y(x+\tau_m)\ -\bar{y})}{\tau_x \qquad \tau_y} \qquad 3.1.4$$

where σ_x is the standard deviation of x about $\bar{x}$, given by

$$\sigma_x = \sqrt{\frac{1}{N-1}\sum_{K=1}^{N} (x(K)-\bar{x})^2} \qquad 3.1.5$$

σ_y is the standard deviation of y about $\bar{y}$, given by

$$\sigma_y = \sqrt{\frac{1}{N-1}\sum_{K-1}^{N} (y(K)-\bar{y}^2)} \qquad 3.1.6$$

N is the number of data points,

$_m$ is the mth time lag or lead.

Another popular numerical analysis technique is to expand digital data on a Fourier Series. Data that is periodic in time is especially well suited to Fourtier analysis. Any well behaved function satisfying the Dirichlet conditions can be expanded in a Fourier Series. For a function, x(t), the Fourier Series is given by

$$x(t) = \frac{a_o}{2} + \sum_{n=1}^{\infty} a_n \cos\frac{n\pi t}{T} + b_n \sin\frac{n\pi t}{T} \qquad 3.1.7$$

where

$$a_n = \frac{2}{T}\int_o^{2T} dt\ x(t)\ \cos\frac{n\pi t}{T} \qquad 3.1.8$$

and

$$b_n = \frac{2}{T}\int_o^{2T} dt\ x(t)\ \sin\frac{n\pi t}{T} \qquad 3.1.9$$

Similar to the case with the cross correlation function, digital data can be adapted to the exact expression in the following manner:

$$a_n = \frac{1}{N} \sum_{K=1}^{N} x(K) \cos \frac{K\Delta tn\pi}{T} \qquad 3.1.10$$

$$b_n = \frac{1}{N} \sum_{K=1}^{N} x(K) \sin \frac{K\Delta tn\pi}{T} \qquad 3.1.11$$

Analytical expressions for the phase and gain of the transfer function are given in sections 2.1 and 2.2. Estimating these parameters from numerical data will be described, because this is the means by which experimental data is made meaningful. In order to accurately represent a set of digital data with a Fourier Series without taking an infinite number of frequencies, it is necessary to cut off the sum in equation 3.1.7 at a certain point. This point, known as the Nyquist frequency is given by (Thie, 1981),

$$f_n = \frac{N}{2T} \qquad 3.1.12$$

The phase of the transfer function can be interpreted as the time lag or lead by which the system responds to a perturbation. In the case of the nuclear reactor being driven by a reactivity perturbation, the phase is given by the time lag of the neutron population. Figure 2 shows the reactor power and reactivity as a

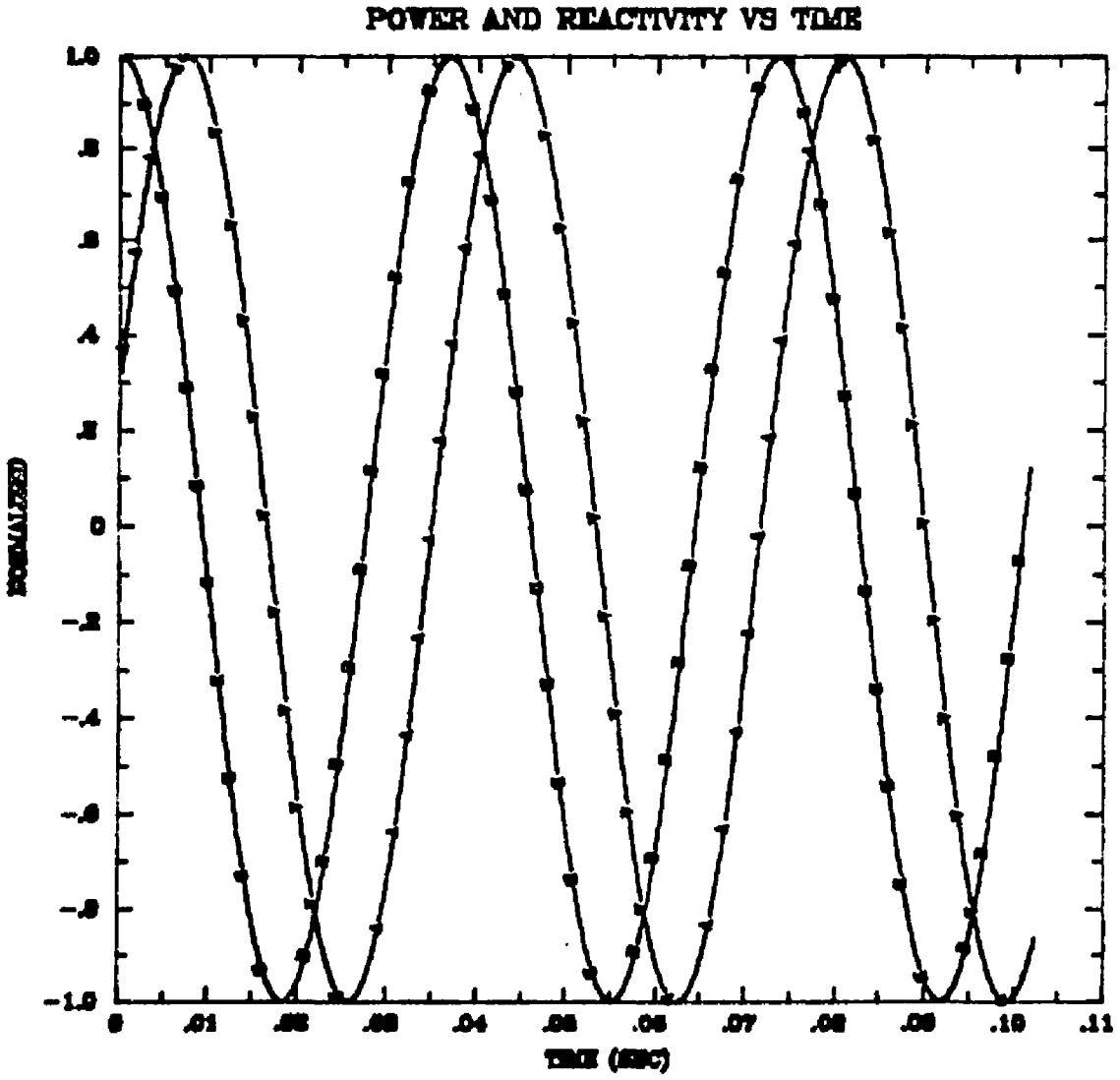

A: Reactivity
B: Power

Figure 2. Reactivity and power versus time.

as a function of time illustrating the phase lag for ω-96 rad/sec. ρ_o=-$0.19. By substituting equation 2.2.18 into equation 3.1.4 for the cross-correlation function, it can be shown that $\phi xy=1$ for $\tau_m=-\phi$. Therefore, by analyzing digital power versus time data with reactivity versus time data, the phase as a function of frequency can be found, by shifting τ_m until ϕxy is a maximum.

Since the gain of the transfer function is a measure of the amplitude of the power oscillation, it can be found digitally by calculating the standard deviation about the mean for one cycle of power versus time, using equation 3.1.5.

CHAPTER 4

SAFEGUARDS APPLICATIONS OF DYNAMIC MEASUREMENTS

Traditional safeguards analysis involved using a steady state measurement of the neutron population in a sample. Two drawbacks associated with this technique are (1) all information about spatial dependence is lost, and (2) since all neutrons "look the same," to a given detector, the sources of neutrons are indistinguishable. A fundamental difference between fissile species is the delayed neutron fractions and halflifes. By performing a dynamic measurement of the neutron population, the differences in the delayed neutron properties and their relative effect can be seen. Table 1 shows the delayed neutron data for U-235 and Pu-239.

Two of the parameters that can be realized from the measurements described are the fractions of fissile isotopes and the local neutronic properties of the medium. The theoretical considerations necessary to arrive at this information will be described.

Table 1. Delayed neutron data for U-235 and Pu-239.*

Group	Half-Life	β_i
Delayed neutron data for U-235		
1	54.51s	0.000243
2	21.84	0.001363
3	6.00	0.001203
4	2.23	0.002605
5	0.496	0.000819
6	0.179	0.000166
Delayed neutron data for Pu239		
1	53.72	0.000076
2	22.29	0.000560
3	5.19	0.000432
4	2.09	0.000656
5	0.549	0.000206
6	0.216	0.000070

*From Introduction to Nuclear Reactor Theory, by John Lamarsh (Addison Wesley Publishing Co., 1965).

Equations 2.2.1 and 2.2.2 were derived from diffusion theory assuming one source of fission neutrons and delayed neutron precursors. Define a quantity, Ψ_{25} as the fraction of fission due to fission of U-235 and Ψ_{49} the corresponding fraction of fissions due to Pu-239. Substituting these definitions into the diffusion equation and deriving the point reactor kinetic equations gives

$$\frac{dn}{dt} = \frac{\rho-\beta_{eff}}{\ell} n + \Psi_{25} \sum_{i=1}^{6} \lambda i \, ci \Big|_{U\text{-}235} + \Psi_{49} \sum_{i=1}^{6} \beta i \, ci \Big|_{Pu\text{-}239} \qquad 4.1.1$$

$$\frac{dci}{dt}\Big|_{U\text{-}235} = \frac{\beta i}{\ell} n - \lambda i \, ci \Big|_{U\text{-}235} \qquad 4.1.2$$

$$\frac{dci}{dt}\Big|_{Pu\text{-}239} = \frac{\beta i}{\ell} n - \lambda i \, ci \Big|_{Pu\text{-}239} \qquad 4.1.3$$

Following through the derivation of section 2.2 with the modified equations gives

$$\tan \phi = \frac{-\omega(\ell+\Psi_{25} \sum_{i=1}^{6} \frac{\lambda i \, \beta i}{\lambda_i 2 + \omega^2} + \Psi_{49} \sum_{i=1}^{6} \frac{\lambda i \, \beta i}{\lambda i^2+\omega^2}}{\beta - \rho_o - \Psi_{25} \sum_{i=1}^{6} \frac{\lambda i^2 \beta_i}{\lambda_i 2+\omega^2} - \Psi_{49} \sum_{i=1}^{6} \frac{\lambda i^2 \beta i}{\lambda i^2+\omega^2}} \qquad 4.1.4$$

By using equation 4.1.4, any correction for effective delayed neutron fractions cancel out. The phase of the reactor transfer function as a function of frequency can be measured and Ψ_{25} and Ψ_{49} can be found by least squares fitting the data equation 4.1.4.

Figures 3 and 4 show how the reactor transfer function is affected by varying concentration of U-235 and Pu-239

Local Perturbations

Up to this point, it has been assumed that the fuel material can be described by a point, that is, there is no spatial flux distribution. Although this is a useful approximation in some situations, a large amount of information about local neutronic characteristics is lost. However, the time and space dependent, heterogeneous diffusion equation is a difficult equation to solve. In view of this, it is suggested that a less complicated descriptor consisting of a hybrid of point reactor kinetics and one-group diffusion theory be used. This combination uses point reactor kinetics to describe the global response of the fuel material and one-group diffusion theory to describe how the local reactivity oscillation affects the reactor. The restrictions imposed by using point reactor kinetics and one-group diffusion can be summarized as

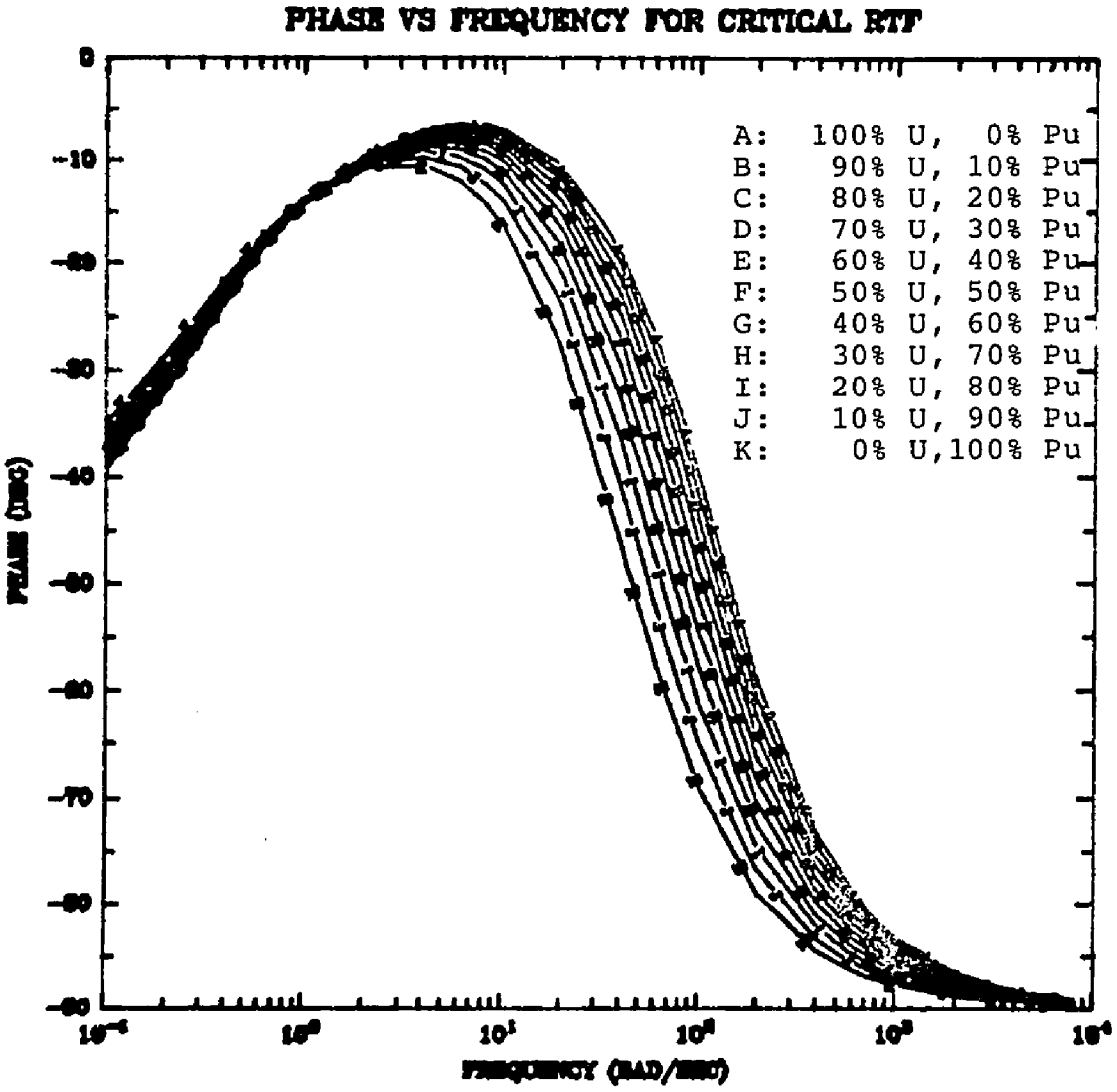

Figure 3. Phase of reactor transfer function versus frequency for critical reactor with varying concentration of Pu-239.

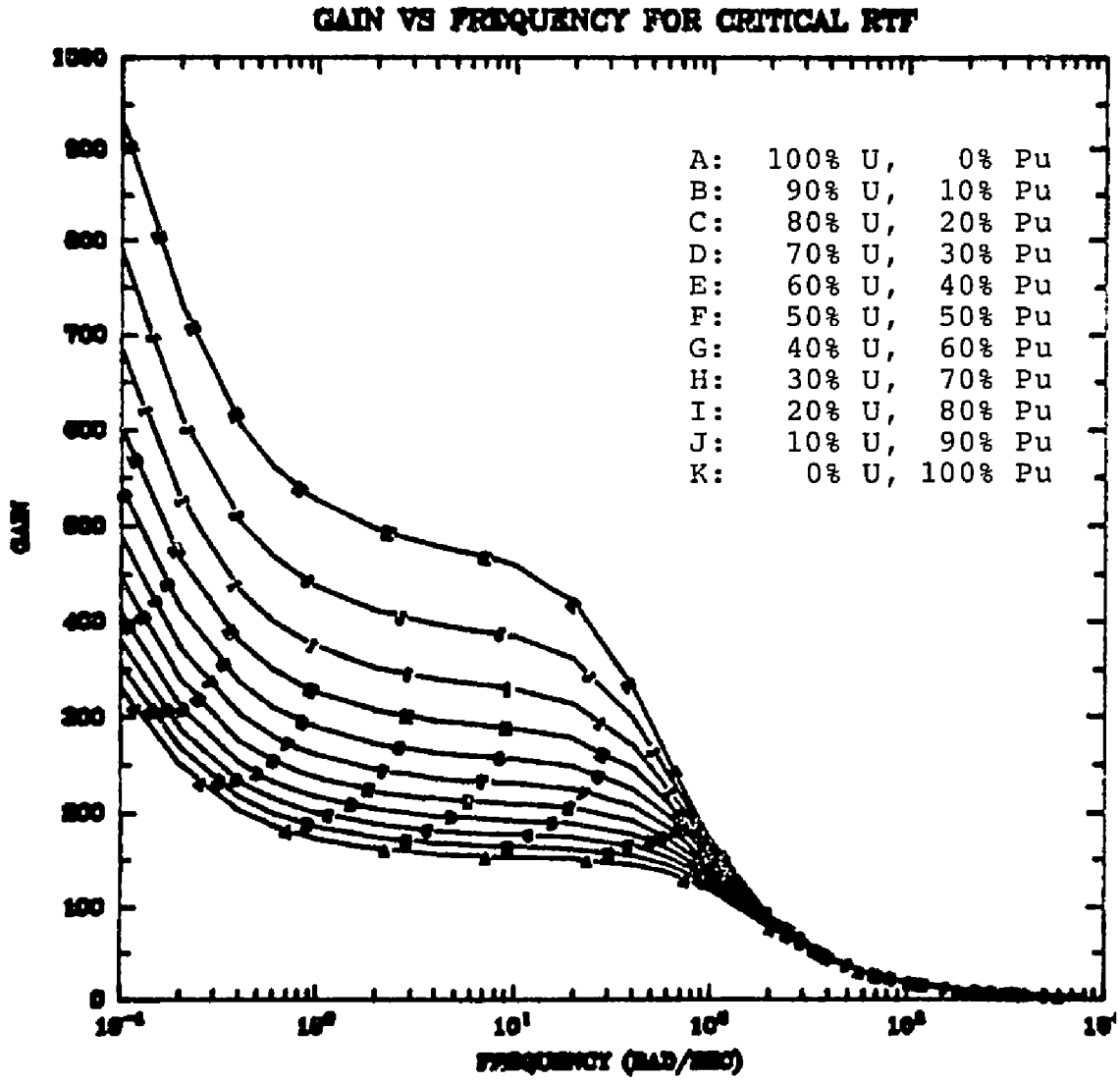

Figure 4. Gain of reactor transfer function versus frequency for critical reactor with varying concentration of Pu-239.

follows. For one-group diffusion theory to be valid, the region being analyzed must be away from boundaries and not strongly absorbing. To use point reactor kinetics, the reactor must indeed behave as a point, that is, there can be no spatial dependence in the response. In light of these unphysical restrictions, the theory provides a good explanation and predicts amazingly accurate results.

This effect can be analyzed analytically. From steady state one-group diffusion theory,

$$D \nabla^2 \phi + (\nu\Sigma_f - \Sigma_a) \phi = 0 \qquad 4.2.1$$

For the time dependent case,

$$D \nabla^2 \phi^1 + (\nu^1\Sigma^1_f - \Sigma^1_a) \phi^1 = \frac{1}{v} \frac{\partial \phi^1}{\partial t} \qquad 4.2.2$$

Assume the neutron population can be expanded in a Fourier Series, and that it is separable in time and space. This gives

$$\phi^1 = \phi_o (r,t) \phi^1 (t) \qquad 4.2.3$$

and

$$\phi^1(t) = \frac{a_o}{2} + \sum_{N=1}^{\infty} (a_n \cos \frac{n\pi t}{T} + b_n \sin \frac{n\pi t}{T}) \qquad 4.2.4$$

Taking derivitatives of equation 4.2.4 with respect to time gives,

$$\frac{\partial \phi^1}{\partial t} = \sum_{n=1}^{\infty} \frac{n\pi}{T} (b_n \cos \frac{n\pi t}{T} - a_n \sin \frac{n\pi t}{T}) \qquad 4.2.5$$

Substituting, and neglecting time derivitives of $\phi(r,t)$,

$$D\nabla^2\phi_o + (\nu^1\Sigma_f - \Sigma_a^1 - \frac{1}{v}\frac{\sum_{n=1}^{\infty}\frac{n\pi}{T}(b_n\cos\frac{n\pi t}{T} - a_n\sin\frac{n\pi}{T})}{\frac{a_o}{2} + \sum_{n=1}^{\infty}(a_n\cos\frac{n\pi t}{T} \quad Tb_n \sin\frac{n\pi t}{T}}) x \quad \phi_o = 0 \qquad 4.2.6$$

Now, assume

$$\nu^1 = \nu + \Delta\nu \qquad 4.2.7$$

$$\Sigma_f^1 = \Sigma_f + \delta\Sigma_f \qquad 4.2.8$$

$$\Sigma_a^1 = \Sigma_a + \delta\Sigma_a \qquad 4.2.9$$

Substituting, and neglecting second order products gives,

$$D\nabla^2\phi_o + (\nu\Sigma_f - \Sigma_a)\phi_o + \left(\nu\partial\Sigma_f + \Delta\nu\Sigma_f - \delta\Sigma_a - \frac{1}{v}\frac{\sum_{n=1}^{\infty}\frac{n\pi}{T}(b_n\cos\frac{n\pi t}{T} - a_n\sin\frac{n\pi}{T}}{\frac{a_o}{2} + \sum_{n=1}^{\infty}a_n\cos\frac{n\pi t}{T} + b_n\sin\frac{n\pi t}{T}}\right) \quad \phi_o = 0 \qquad 4.2.10$$

Define the operators M and P such that

$$M = \nabla^2 + (\nu\Sigma_f - \Sigma_a) \qquad 4.2.11$$

and

$$P = \nu\delta\Sigma_f + \Delta\nu\,\Sigma_f - \delta\Sigma_a +$$

$$-\frac{1}{v}\;\frac{\sum_{n=1}^{\infty}\frac{n\pi}{T}\left(b_n\cos\frac{n\pi t}{T} - a_n\sin\frac{n\pi t}{T}\right)}{\frac{a_o}{2} + \sum_{n=1}^{\infty} a_n\cos\frac{n\pi t}{T} + b_n\sin\frac{n\pi t}{T}} \qquad 4.2.12$$

Assume that an adjoint function exists such that

$$M\Psi = 0 \qquad 4.2.13$$

Substituting 4.2.11 and 4.2.12 into 4.1.10 gives

$$(M+P)\;\phi_o = 0 \qquad 4.2.14$$

Multiply equation 4.2.14 by ϕ_o and equation 4.2.14 by Ψ, subtract one from the other and integrate over the reactor core.

$$\int_v (\Psi\;(M+P)\;\phi_o - \phi_o\;M\;\Psi)\;dv = 0 \qquad 4.2.15$$

Since Ψ is adjoint to ϕ_o, expanding 2.4.15 gives

$$\int_v \Psi P\;\phi_o\;dv = 0 \qquad 4.2.16$$

Substituting 4.2.12 into 4.2.16 gives

$$\int_v \Psi\left(\nu\delta\Sigma_f + \Delta\nu\Sigma_f - \delta\Sigma_a - \frac{1}{v}\;\frac{\sum_{n=1}^{\infty}\frac{n\pi}{T}\left(b_n\cos\frac{n\pi t}{T} - a_n\sin\frac{n\pi t}{T}\right)}{\frac{a_o}{2} + \sum_{n=1}^{\infty} a_n\cos\frac{n\pi t}{T} + b_n\sin\frac{n\pi t}{T}}\right)\phi_o\,dv = 0 \qquad 4.2.17$$

Define the effective change in reactivity by,

$$\rho = -\frac{\Delta\nu}{\nu} \qquad 4.2.18$$

and rearranging 4.2.17 gives

$$\rho = -\frac{\int_v^{\psi} \nu\delta\Sigma_f - \delta\Sigma_a \frac{1}{v} \frac{\sum_{n=1}^{\infty} \frac{n\pi}{T}\left(b_n \cos\frac{n\pi t}{T} - a_n \sin\frac{n\pi t}{T}\right)}{\frac{a_o}{2} + \sum_{n=1}^{\infty} \cos\frac{n\pi t}{T} + b_n \sin\frac{n\pi t}{T}} \phi_o dv}{\nu\int_v \psi\Sigma_f \quad \phi dv} \qquad 4.2.19$$

If the change in reactivity is introduced by inserting non-fissile absorber, $\delta\Sigma_f = 0$. Also it can be shown that for an unreflected reactor, $\Psi\alpha\phi_o$. For a small sized absorber, assuming $\Psi\alpha\phi_o$ represents the same order approximation as the linearization assumption used to derive the kinetics equations.

Substituting,

$$\rho = C \int_v \phi^2 \left(\delta\Sigma_a + \frac{1}{v} \frac{\sum_{n=1}^{\infty} \frac{n\pi}{T}\left(b_n \cos\frac{n\pi t}{T} - a_n \sin\frac{n\pi t}{T}\right)}{\frac{a_o}{2} + \sum_{n=1}^{\infty} \left(a_n \cos\frac{n\pi t}{T} + b_n \sin\frac{n\pi t}{T}\right)}\right) dv \qquad 4.2.20$$

where C is a constant.

By Fourier analyzing the data, the constants a_n and b_n can be obtained, thereby giving a value for the relative reactivity as a function of angular position. If no perturbations exist, the reactivity as a function of angle will be as in Figure 5, perfectly sinusoidal. For the case with no feedback, other frequencies will indicate perturbations in the flux at the corresponding angle.

From equation 4.2.20, the reactivity is proportional to the square of the local flux. Figure 6 shows how the reactor power will follow the motion of the oscillator as it moves into and out of regions of higher flux. Now assume that something is near the reactivity oscillator that will change the flux. From equation of 4.2.20, this will cause a change in the net worth of the oscillator when it nears the region of perturbed flux. This change is further modified by the lag of the reactor power with respect to the oscillator position.

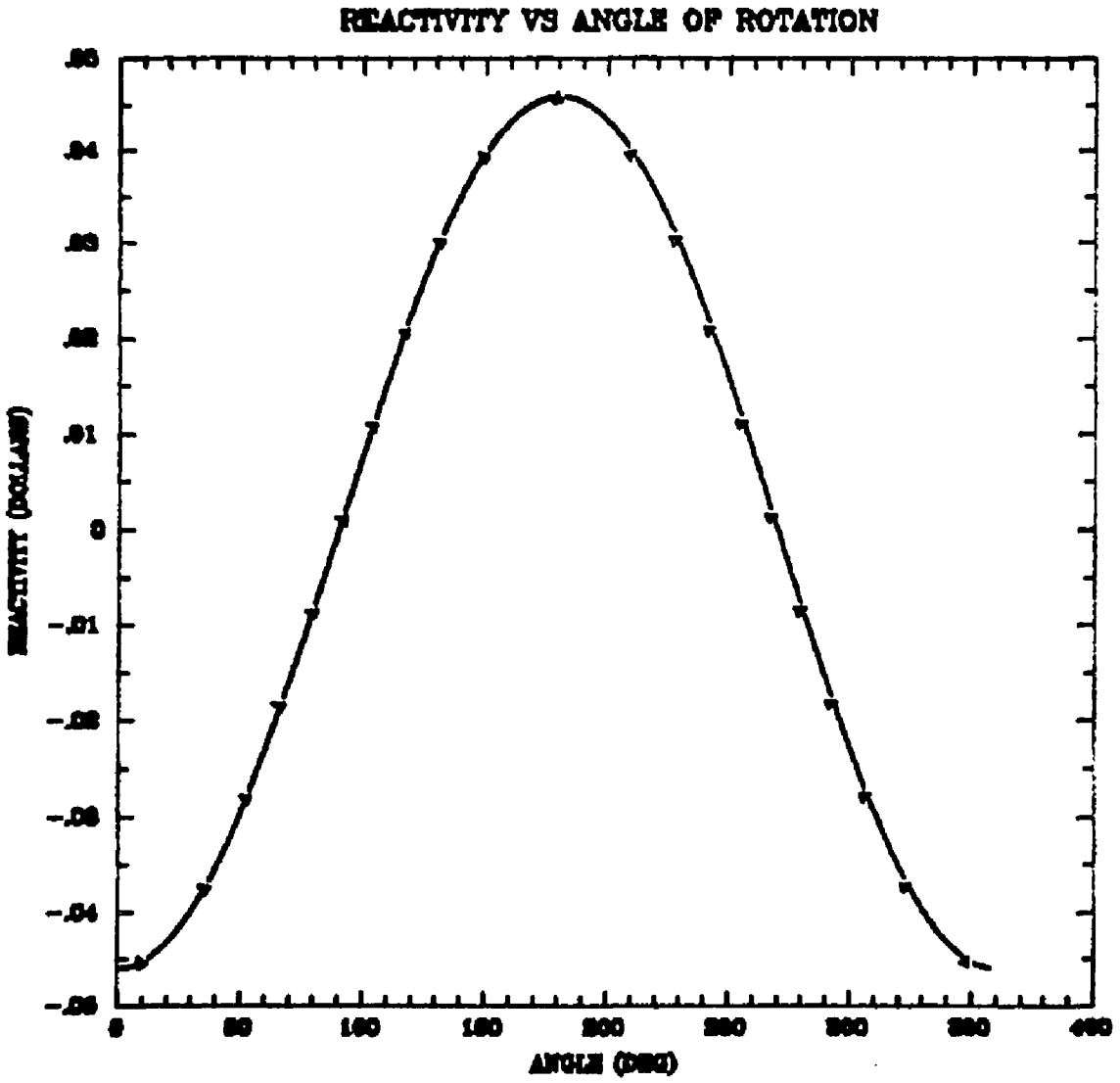

Figure 5. Reactivity versus angle of rotation for rod oscillator.

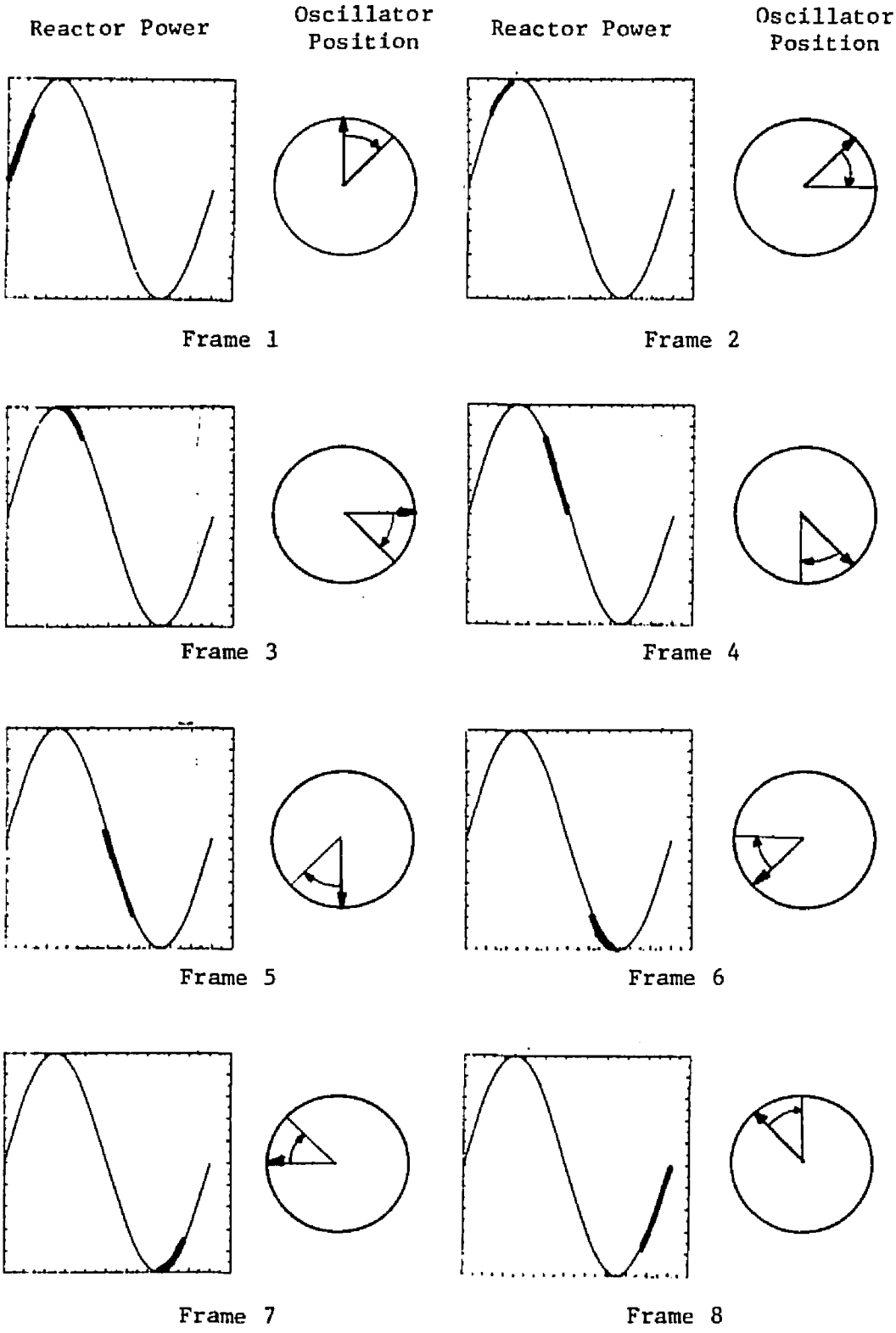

Figure 6. Position of oscillator and reactor power.

CHAPTER 5

EXPERIMENT

An experiment was designed to test the analytical expressions derived. The reactor used was The University of Arizona TRIGA Research Reactor. The reactor is a TRIGA Mark I reactor fueled with standard TRIGA fuel. There is a 12" radial graphite reflector on the core. The core configuration is the standard configuration, denoted S-21, having low burnup and high burnup fuel randomly dispersed throughout the 87 fuel locations. By measuring the gain and phase of power oscillations, values for the fractions of U-235 and Pu-239 can be found. Also, any local perturbations in the flux can be detected.

By forcing the reactor power to oscillate, measurements of the gain and phase of the reactor transfer function can be made to estimate the parameters described in Section 4. Two methods can be used to force oscillations; a changing source strength or a changing reactivity. Changing source strength is useful for subcritical assemblies, and even in this region, severe drawbacks exist. Several attempts at measurements of source transfer function are described in the Appendix. Reactivity

oscillations are the common choice. One type of reactivity oscillator is shown in Figure 7. The cadmium strip, being a strong thermal neutron absorber introduces oscillations in the reactor power which can then be measured.

Equipment

A strip of cadmium within an aluminum tube (the rod oscillator) was inserted in an empty fuel element location in the outer fuel ring of the core. The strip of cadmium was attached to a drive motor, the speed of which was varied using a set of pulleys. A power versus time trace was obtained by signal input from a compensated ion chamber and a BF3 tube to a multi-channel analyzer in the multi-channel scaling mode. The start of the trace was synchronized with a timing wheel attached to the shaft connecting the motor and the cadmium strip. Figure 8 is a block diagram of the data acquisition equipment. Figure 7 is a diagram of the rod oscillator unit.

Procedure

The reactor was brought to a critical condition below the feedback region and above the point where electronic noise would affect the automatic controller. The reactor was then put into the automatic mode and allowed to stabilize. The rod oscillator was then turned manually in 10° increments to find the reactivity as a

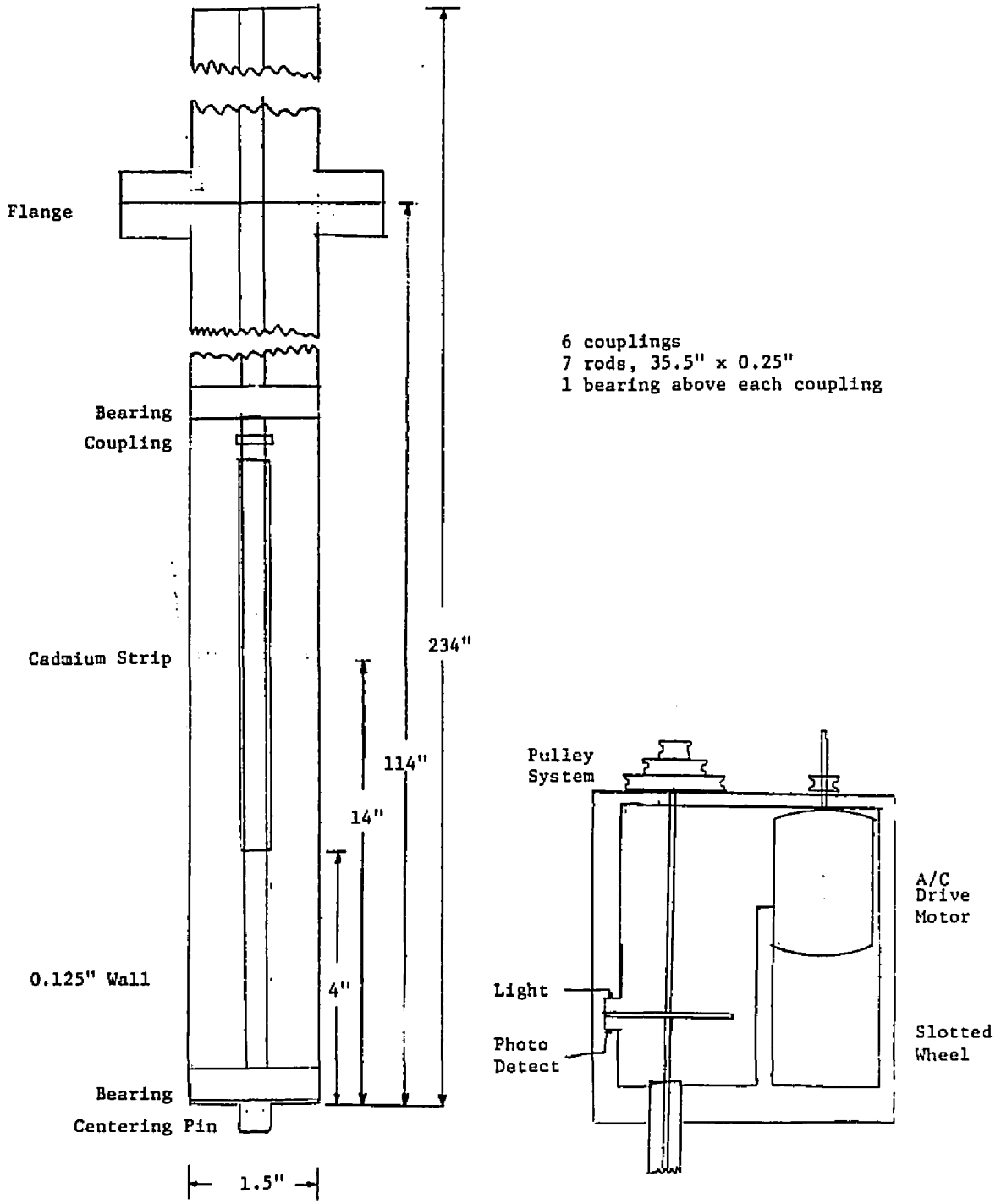

Figure 7. Rod oscillator and rod oscillator drive unit.

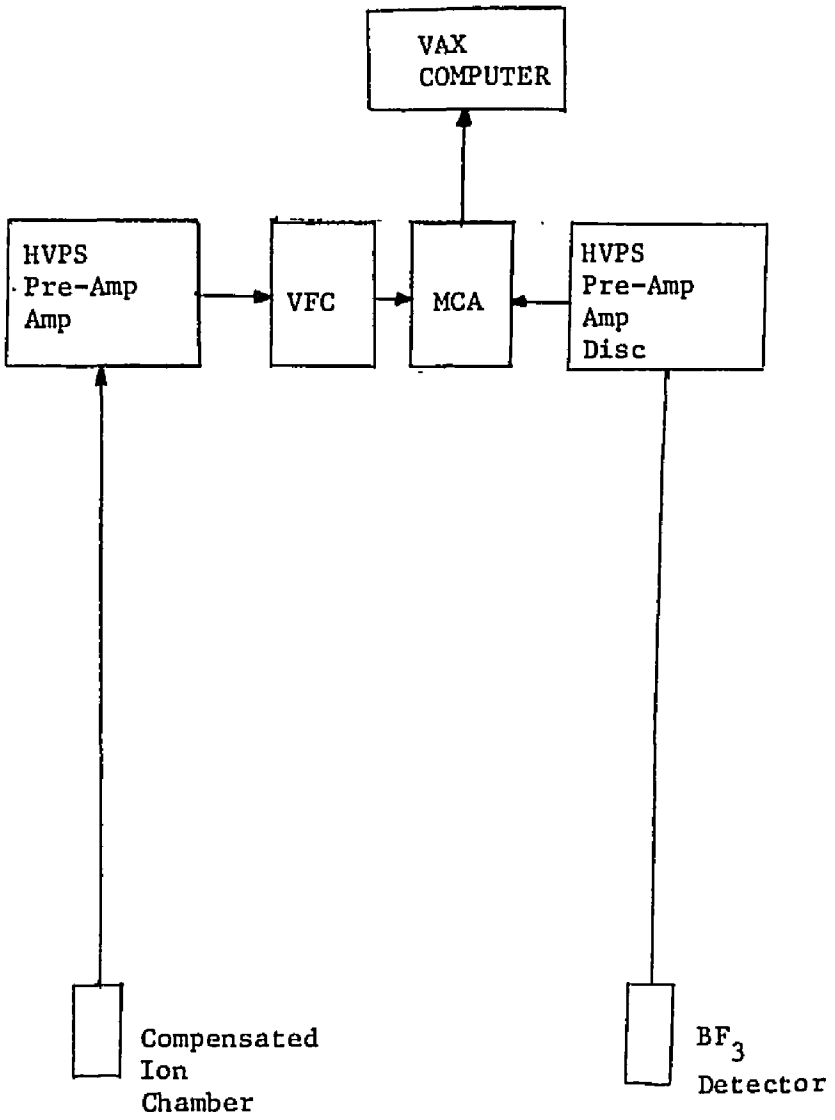

Figure 8. Block diagram of the data acquisition equipment.

for incremental worths. The data was least-squares fitted to the equation.[1]

$$\rho = A_1 \sin (\omega t + A_2)$$

The phase angle, A2, gives the phase lag of the reactivity with respect to the initiation of the timing pulse. The power versus time data were then least-squares fitted to the equation

$$n = C_1 \sin (\omega t + C_2) + C_3$$

The phase angle, C2, gives the phase lag of the power with respect to the initiation of the timing pulse. Therefore, by comparing A2 and C2 the phase shift can be found. This was accomplished by entering the data from the BF3 into a cross correlating routine and by numerical comparison for the VFC data. The net phase shifts and corresponding frequencies were then entered into a routine that fit the phase and frequency to equation 4.1.4. The power versus time data was Fourier analyzed to find the Fourier coefficients and the constants where substituted into equation 4.2.20.

Because it is not possible to measure the neutron generation time independently of the delayed neutron fraction, the parameter β/ℓ was measured. Also, because of the effective higher worth of the delayed neutrons, the

[1] Codes written by author.

function of angular position as well as the maximum reactivity swing. The pulley system was set up at the desired frequency and the motor started, with the oscillator initially in its time averaged zero worth position. The timing signal from the rod oscillator was input to the sweep trigger of the multi-channel analyzer (MCA). This would synchronize the start of the MCA sweep with the starting position of the rod oscillator. This signal was also input to a counter, to give the number of cycles per second. The MCA was put into the recycle mode with a time per channel setting such that approximately two cycles were recorded in one sweep (1024 channels). After about 30000 counts per channel were recorded in the peaks, the MCA was stopped, and the contents of the memory were dumped into the permanent memory of a VAX computer, for data reduction. The pulley system was changed to give a different frequency, the MCA reset, and another measurement taken. After a complete set of data was obtained for a given core configuration, fuel was moved and the process repeated.

Data Reduction

Using the position of the timing wheel that gives the trigger signal as the reference position, the reactivity as a function of angular position was determined for the oscillator, using control rod calibration tables

effective delayed neutrons fractions are not known. This drawback can be eliminated by using the expressions for the phase of the transfer function as a measured parameter, and assuming that all the delayed neutrons are born at the same energy. By rearranging the equation 4.1.4, the only parameters to be measured are β/ℓ and ϕ and values of β_i/β can be looked up in the literature.

Results and Discussion

The data from the BF3 detector and the compensated ion chamber were analyzed to find a value of β/ℓ. Values of the phase, and corresponding values for frequency and values for β/ℓ were then substituted into a fitting code to find the fractions of uranium and plutonium. It was assumed that the only fissile isotopes were U-235 and Pu-239.

The extremely high quality of the signal from the compensated ion chamber system makes it unnecessary to cross correlate the data with the rod oscillator to find a phase shift. Figure 9 shows the raw data from the compensated ion chamber with ω=171 rad/sec. The phase shift can be found by simply comparing the relative phases. The data from the BF3 must be cross correlated to give a numerical estimate of the phase shift. Figure 10 shows the normalized cross-correlation function for various lag times. Figure 2 shows the relationship

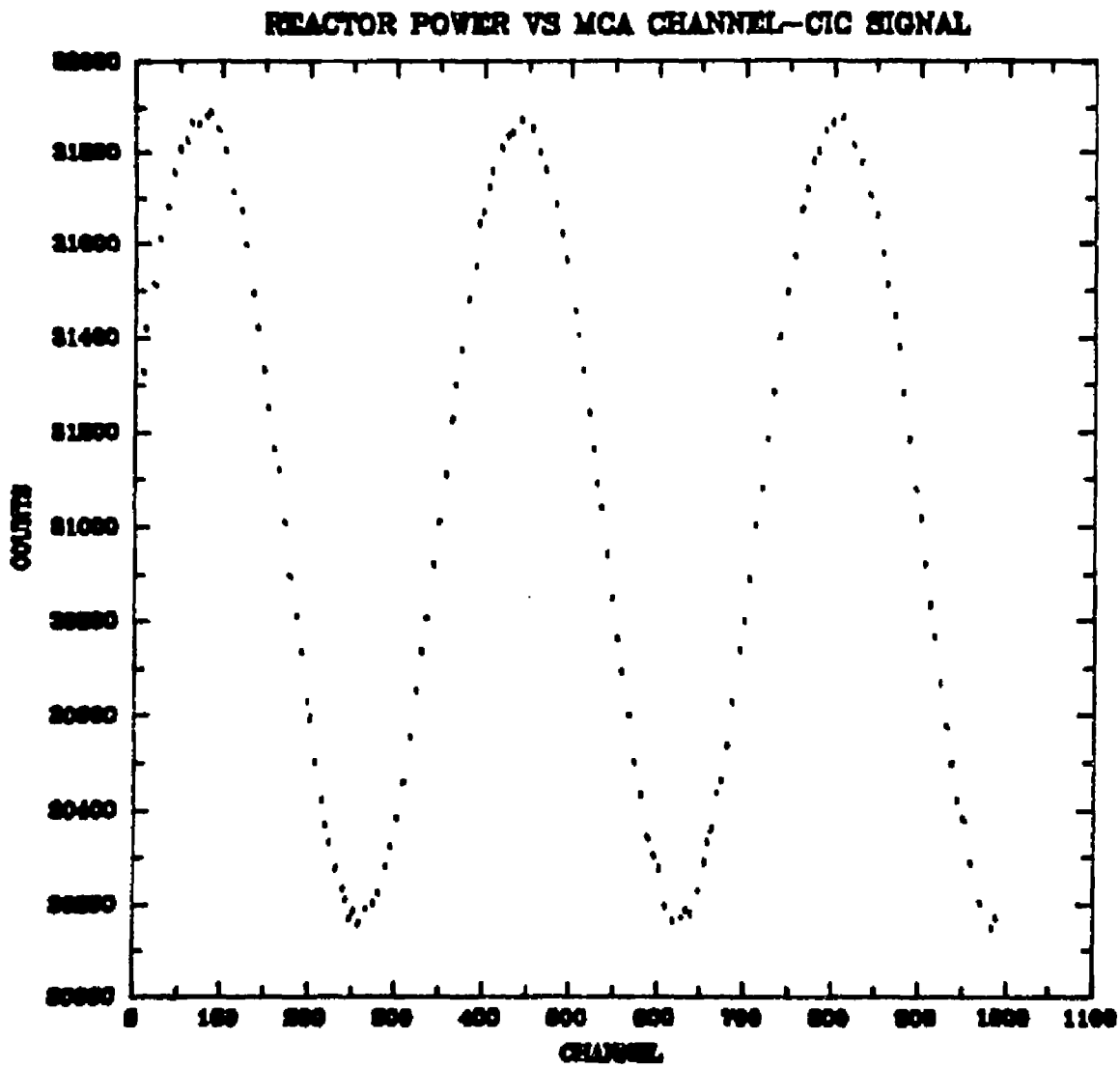

Figure 9. Reactor power versus MCA channel-compensated ion chamber data.

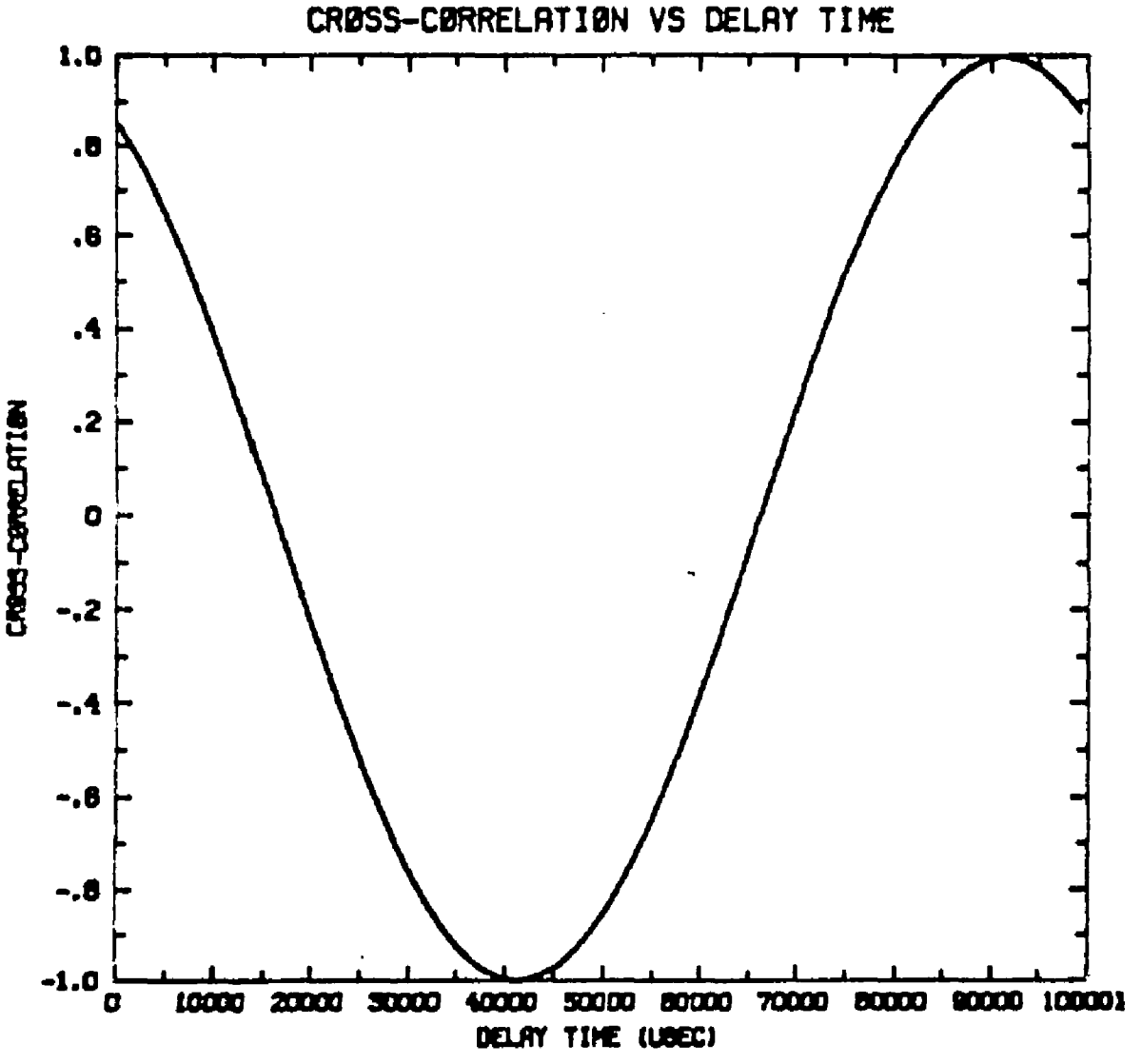

Figure 10. Cross correlation versus delay time.

between reactivity and power. Figures 11 and 12 shows the data and the fitted curves, for a given detector system and core configuration.

As a check and for comparison, the plutonium and uranium content of the core was analyzed using 1-group cross-sections and fluxes. These figures, along with relative peaking factors are tabulated in Table 2. There is reasonable agreement between the two methods. The difference is believed to be due to experimental error and uncertainty in assumed parameters. The burn-up calculation was made for fuel elements with burn-ups as of 7-1-78. Since that time, energy production has resulted in an increase in the Pu-239 concentration of only about 0.5%.

The detection of spatial aberations in the neutron flux is independent of frequency and therefore, requires only a single measurement. Because the data for the U/Pu ratio is the same as that needed to determine spatial flux distributions, many comparisons can be made. Since the oscillator is made of cadmium, it will only be sensitive to perturbations in the thermal flux. Therefore, increased quantities of moderator or fuel will be observed. Figures 13 and 14 show the condition of the core for a given situation. As expected, there is a thermal flux depression in the vicinity of fuel (thermal neutron absorber, fast

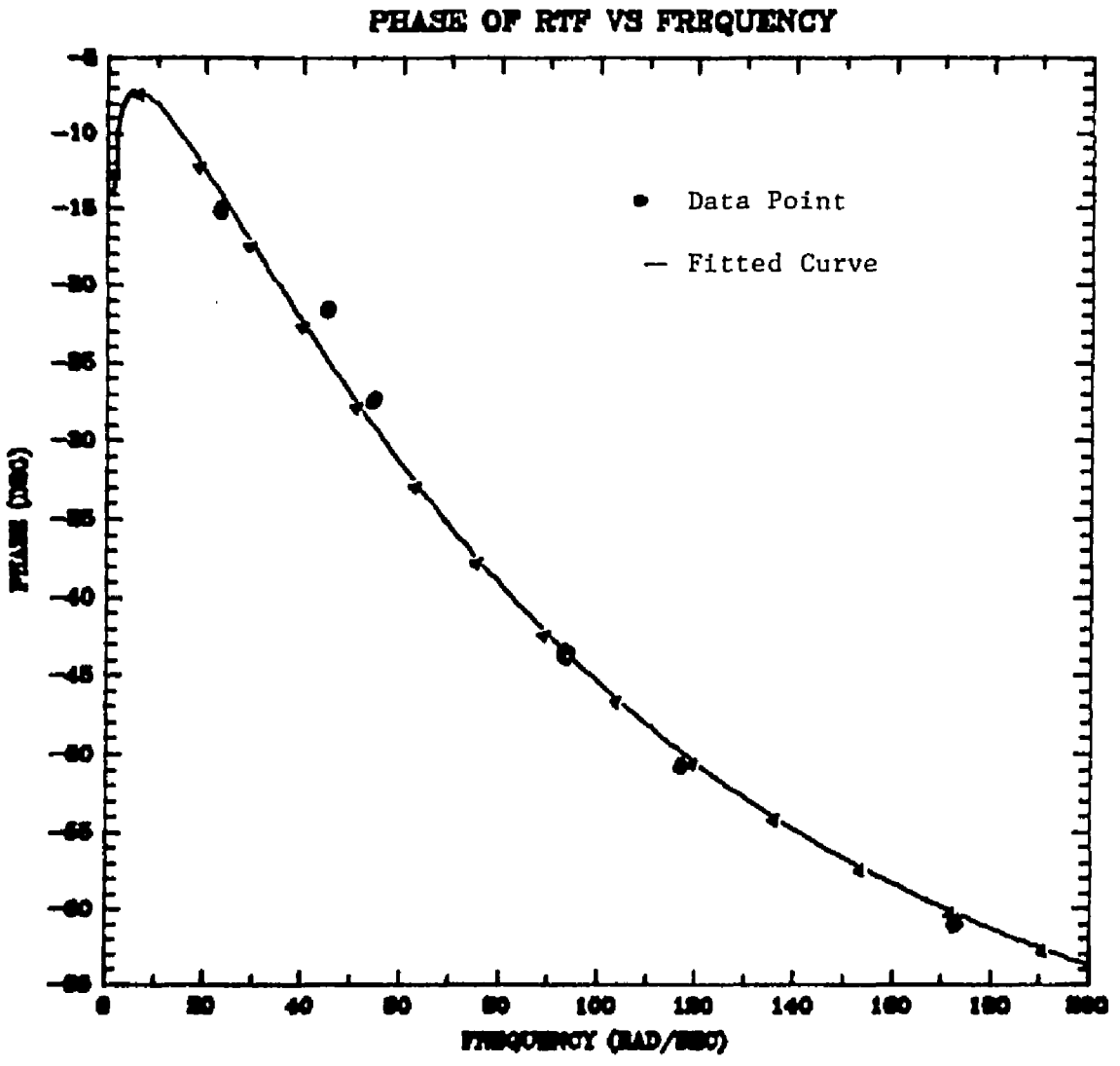

Figure 11. Phase of reactor transfer function versus frequency-fitted curve and data (Experiment 1).

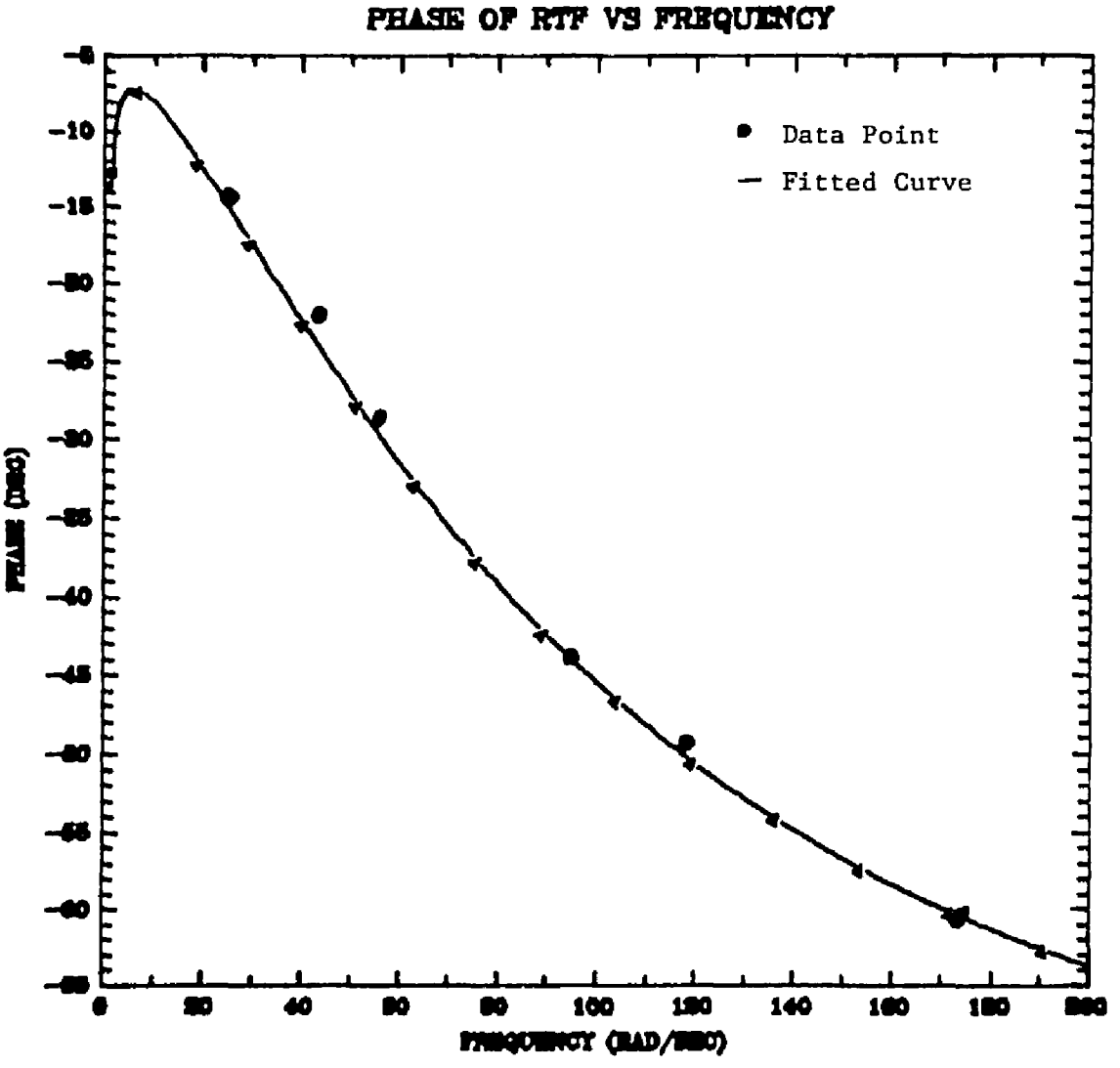

Figure 12. Phase of reactor transfer function versus frequency-fitted curve and data (Experiment 2).

Table 2. Results (Burn-up calculations for isotopic concentrations).

Region of Core	[1]Grams U	[1]Grams Pu	Radial[2] Peaking Factor	Effective Grams U	Effective Grams Pu
B-Ring	215.4	1.40	1.45	312.3	2.04
C-Ring	355.1	2.82	1.39	493.5	3.92
D-Ring	557.1	9.56	1.18	658.5	11.3
E-Ring	801.1	12.1	0.93	745.0	11.2
F-Ring	882.4	15.2	0.70	617.0	10.7
Total				2827.1	39.2
			$\Psi_{25} = 0.9863$	$\Psi_{49} = 0.0136$	

[1]As of 7-1-78

[2]From NE 420 Lab Manual, The University of Arizona.

Measured values: Experiment 1.

$\Psi_{25} = 0.9733 \pm 3.7\%$ $\Psi_{49} = 0.0266 \pm 3.7\%$

Experiment 2.

$\Psi_{25} = 0.9730 \pm 3.7\%$ $\Psi_{49} = 0.0266 \pm 3.7\%$

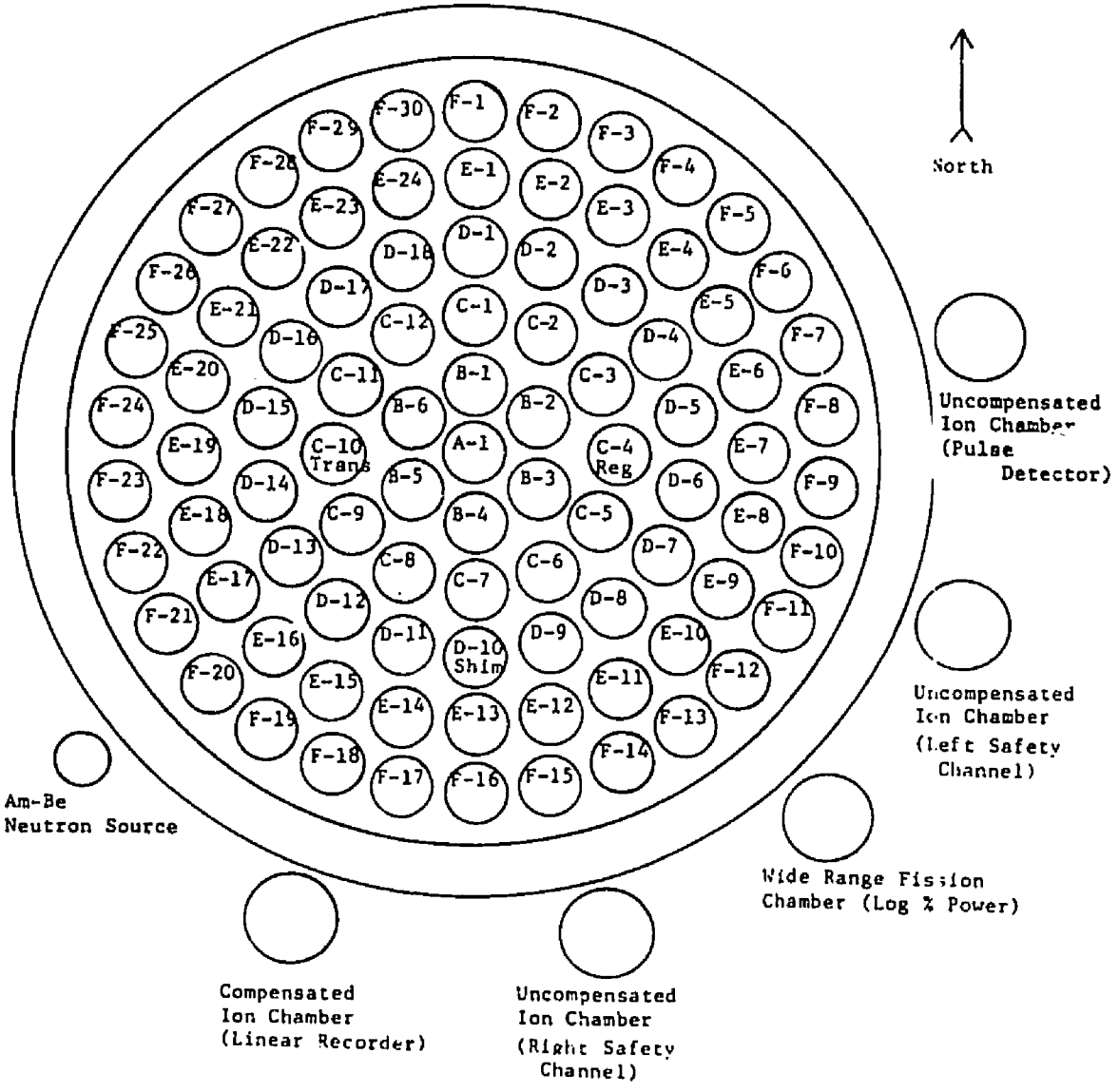

Figure 13. TRIGA core configuration (Experiment 1).

TRIGA CORE CONFIGURATION

EXPERIMENT 2

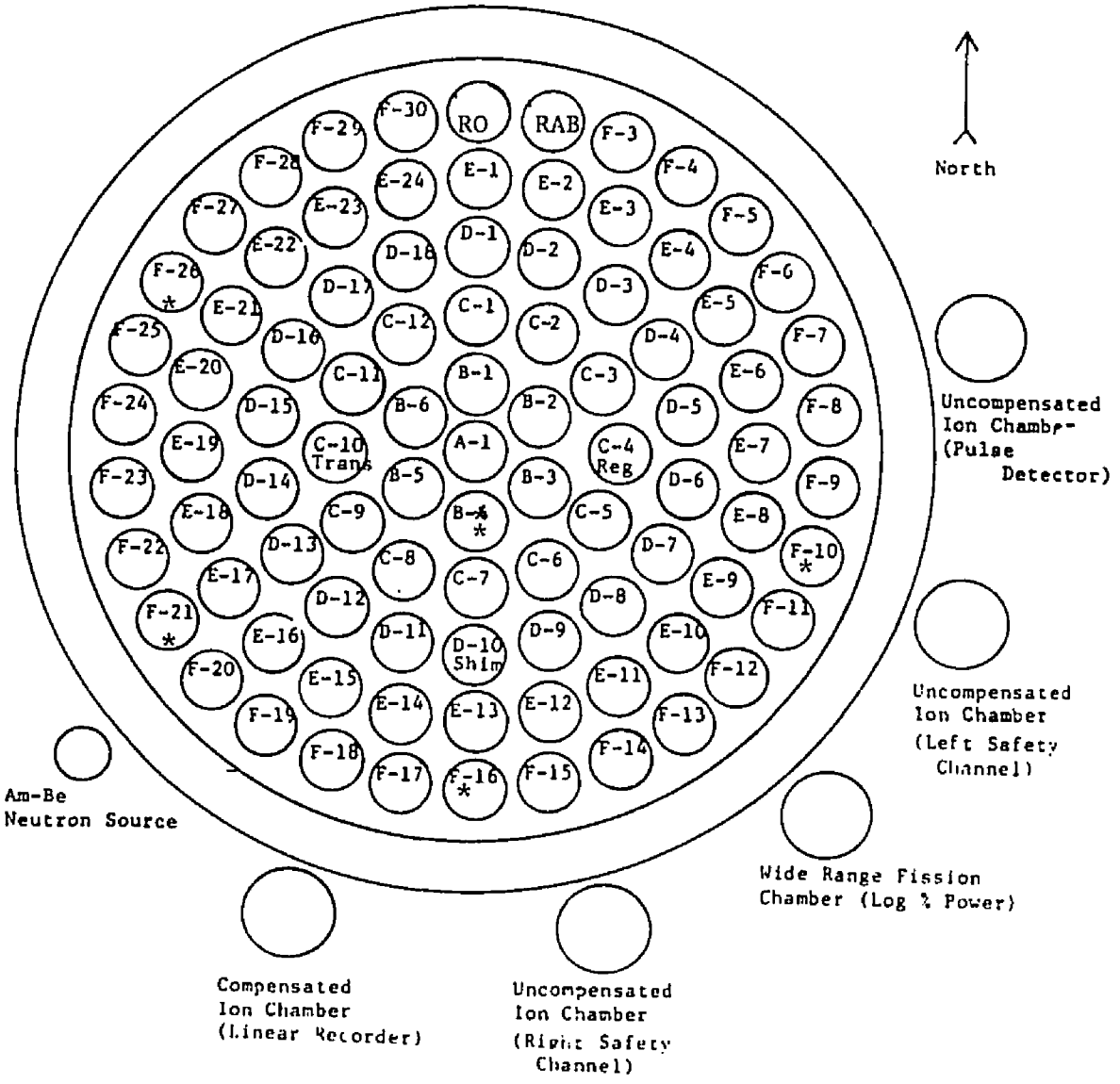

*Indicate where new fuel was replaced.

Figure 14. TRIGA core configuration (Experiment 2).

neutron emitter) and a peaking near large quantities of moderator, water, and graphite.

As shown in Figure 8, data from the compensated ion chamber was input to the MCA via a voltage-to-frequency converter. In the early phase of the experiment, large discrepancies in time were observed. Further investigation led to the discovery that there is approximately a 0.7 mSec time delay in the VFC. Furthermore, this time delay is voltage dependent, becoming larger at lower input voltages and causes the pulses to exhibit a kind of doppler shift and broadening. At low frequencies, 10-20 rad/sec, 1 mSec introduces about a 1.3° phase shift. However, at the high operational frequencies, 150-200 rad/sec, 1 mSec introduces a systematic 10°-15° phase shift. Although the discrepancy can be accounted for and the data adjusted, it introduces unnecessary error and uncertainty. Dead time in the data acquisition systems up to 10 uSec introduces only 1° at the very highest frequencies and therefore, is not a significant problem. Because of the time lag in the VFC system, direct acquisition systems such as BF3 and fission chambers are better for this type of application.

In order to arrive at the results in Table 2, it was assumed that the only error in the measurements was in the phase and the frequency. Errors in the decay

constants and fractions of the delayed neutron precursor groups was left out. Also, it was assumed that the correction for VFC dead time was perfect. Taking those errors into consideration would increase the uncertainty by as much as 15 to 30 percent.

Lag time in the triggering signal was investigated also. Measured delay time in this circuitry were on the order of fractions of a microsecond. At this point, it is believed that most of the systematic error in the project is due to electronic components.

From Figure 5, the percentage of the peak power can be seen as a function of angular position. Figure 4 shows some representative values of gain for various frequencies. Equation 2.2.18 shows the mathematical relationship between gain and power level. Assume $c_1 = 0.03$, $G(iw) = 95$ and oscillator at frame 6 in Figure 5. From this, $n=2.679n_o$. From the derivation of the point-reactor perturbation theory, the reactivity worth of the perturbation goes as the square of the flux, so $\rho eff = 7\rho_{peak}$. So, for a reactivity oscillation of \$0.03 in the steady state, an effective dynamic oscillation of approximately \$0.21 will be observed. Using the prompt jump equation, it can be shown that during a sinusoidal oscillation in reactivity about \$0.0 the power will drift on a period corresponding to $\rho_{drift} = \frac{1}{2} \rho_{peak}^2$.

For the example, described, the reactor power should be on a period of approximately 315 seconds. Figure 15 shows the power as a function of time on the linear channel. Calculating the period shows it to be 313 seconds. From a safeguards standpoint, this phenomena is probably without use, because it says nothing about what is causing the effect. However, from a reactor operations point of view, the implications are far reaching. For example, if the reactor is in a subcritical condition lower than the static maximum swing of reactivity but higher than the dynamic effective swing, the reactor power will increase in an effectively supercritical manner. When the oscillation is stopped, the reactor would return to its subcritical equilibrium power level. This phenomena was in fact observed during the course of this study.

If one assumes the relationship arrived at in Section 4.2 is valid by inserting values of the Fourier coefficients into equation 4.2.20, the angular flux distribution can be found. Figure 16 shows the flux shape. The spikes superimposed upon the sine wave occur near regions of increased thermal flux, near large quantities of water. Although the theory matches the observations, the data is inconclusive. Further experimentation is necessary to determine the exact cause of increased relative worth of the rod oscillator.

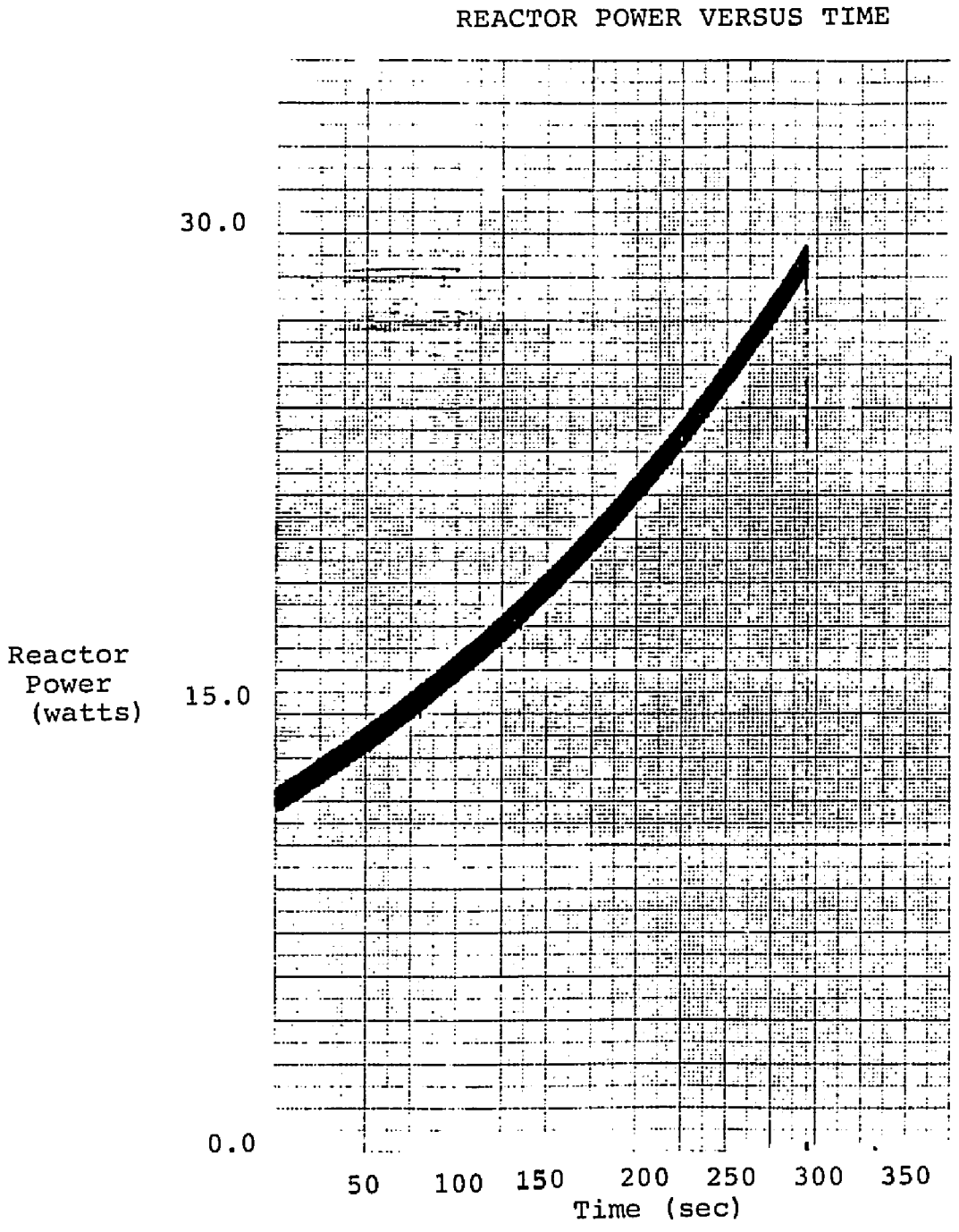

Figure 15. Reactor power versus time-linear channel.

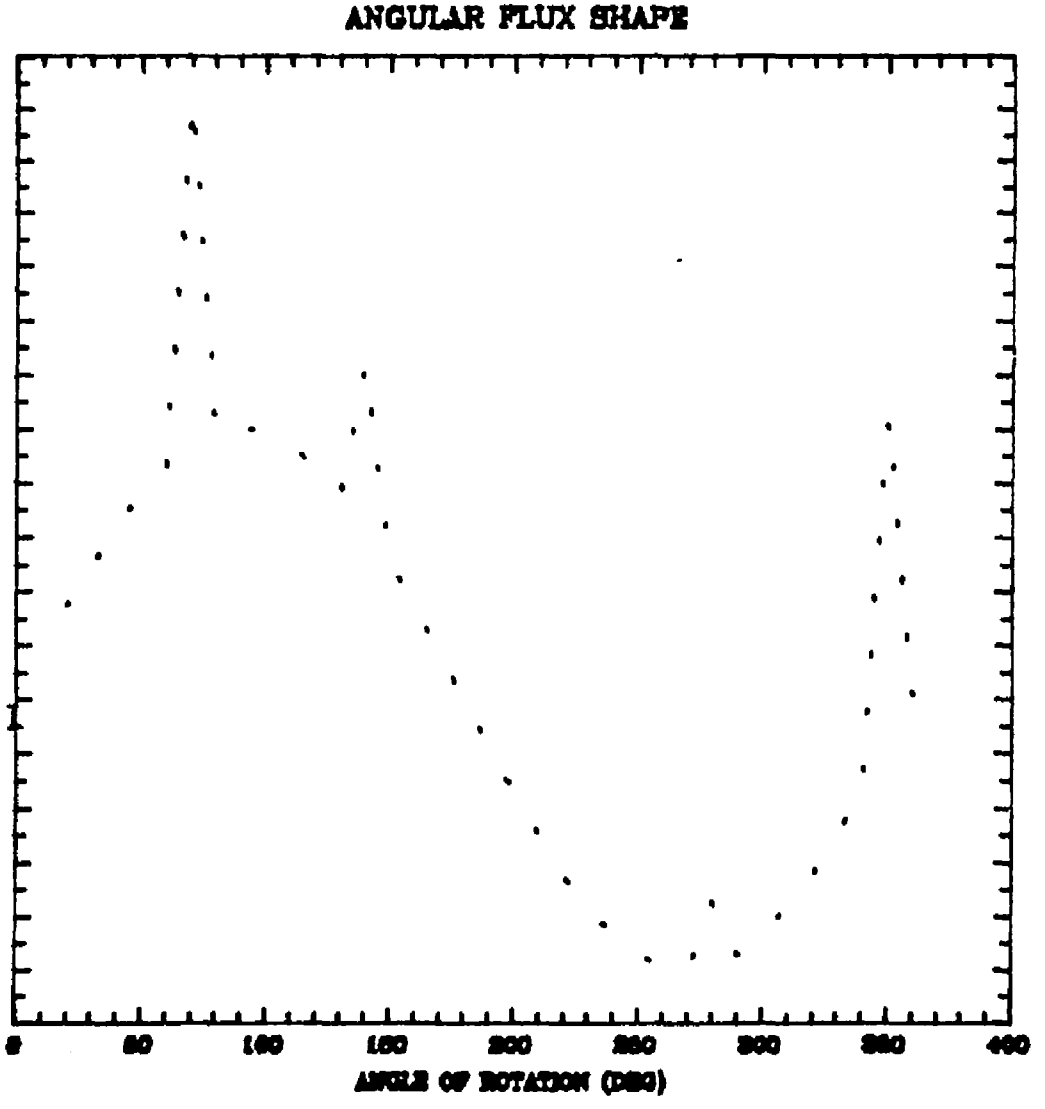

Figure 16. Angular flux shape versus angle of rotation for Experiment 2.

CHAPTER 6

CONCLUSIONS AND RECOMMENDATIONS

A preliminary investigation of the feasibility of using reactivity oscillations to extract safeguards information from The University of Arizona Research Reactor indicated that dynamic measurements of the reactor power provides reasonable information about the fissile content of the reactor core. Although an exhaustive study of the reactivity multiplier effect has not taken place, the one-group point reactor hybrid theory appears to explain the effect and predicts the correct magnitude and location of perturbations in the flux distribution around the reactivity oscillator.

The measurements can be made with a minimum of equipment, and the equipment used is simple in operation and principle. Problems associated with transporting neutron sources or other radioactive materials both domestically and internationally are all but eliminated. Detectors using materials other than special nuclear material can be utilized, eliminating the political implications of transporting SNM. The mechanism is low cost and could potentially be left at the site.

The results of the measurements can be obtained in a short time using a computer. Computing space is a maximum of 32K for a single operation and requires only 500K of storage for all the software and data, easily within the range of todays commercially available microprocessors and bubble storage devices.

It is recommended that further research be carried out in the following areas:

1. Reactivity oscillations with larger fractions of plutonium in the fuel. Because of the low burnup of The University of Arizona TRIGA Fuel, the amount of plutonium in the core is small. It is possible that the information was lost in the statistics of the measurements. Larger, known concentrations of plutonium would prove conclusively the validity of such a measurement.
2. How local perturbations effect the result of the U/Pu ratio. If there is a local change in the worth of the oscillator, linerization assumptions and other second order affects that were neglected may not be valid.
3. Using different detector systems. While discrimination is not important in the reactivity oscillator measurement, in the source transfer function measurements, discrimination of source

and fission neutrons is imperative. It is recommended that Helium-4 tubes and U-238 fission chambers be investigated as possible candidates for detector systems.

4. A further study of the reactivity gain effect. Although the theory described appears to work, several additional experiments need to be run to investigate other possibilities, such as neutron transent times, excitation of a spatial mode or an as of yet undetermined time and space dependent reactivity effect.
5. Application of reactivity oscillations to sub-critical assemblies. Perhaps the most important application of this technique is in the assay of spent fuel assemblies. It has been estimated that spent PWR assemblies have reactivities on the order of -$100. Experimental reactivity oscillations in assemblies with reactivities on the order of that of a spent fuel assembly have not been done, and may not yield useful information.

APPENDIX A

EARLY INVESTIGATIONS

Early attempts at obtaining safeguards information by dynamical measurements were met with limited success. Most of the initial systems involved oscillating a source of neutrons in a sinusoidal manner. The derivation of the source transfer function is identical to the derivation in Section 3.3, except that it is assumed that the reactivity is constant and a sinusoidal source of neutrons exists. Following through the derivation gives a result that is identical with equations 3.2.18, 3.2.19, and 3.2.20, but the small swing restriction has been lifted. Figures 3 and 4 are still applicable also.

Two methods have been developed to produce sinusoidal oscillations in source strength for safeguards analysis. These methods are (1) spinning a source, and (2) constant source behind a rotating sinusoidal "chopper." Figure A1 shows the spinning source type and Figure A2 shows the spinning chopper type. Both of these types have been built and demonstrated with varying degrees of success. The range of usefulness of a given system is directly dependent upon the effective multiplication factor of the assembly being interrogated. Figures A3 and A4 show how the phase and gain are dependent upon the relative reactivity of the system. By extending Figure A3, it can be shown that in order to get phase shifts of 10° for a system with a reactivity of $-100, angular frequencies

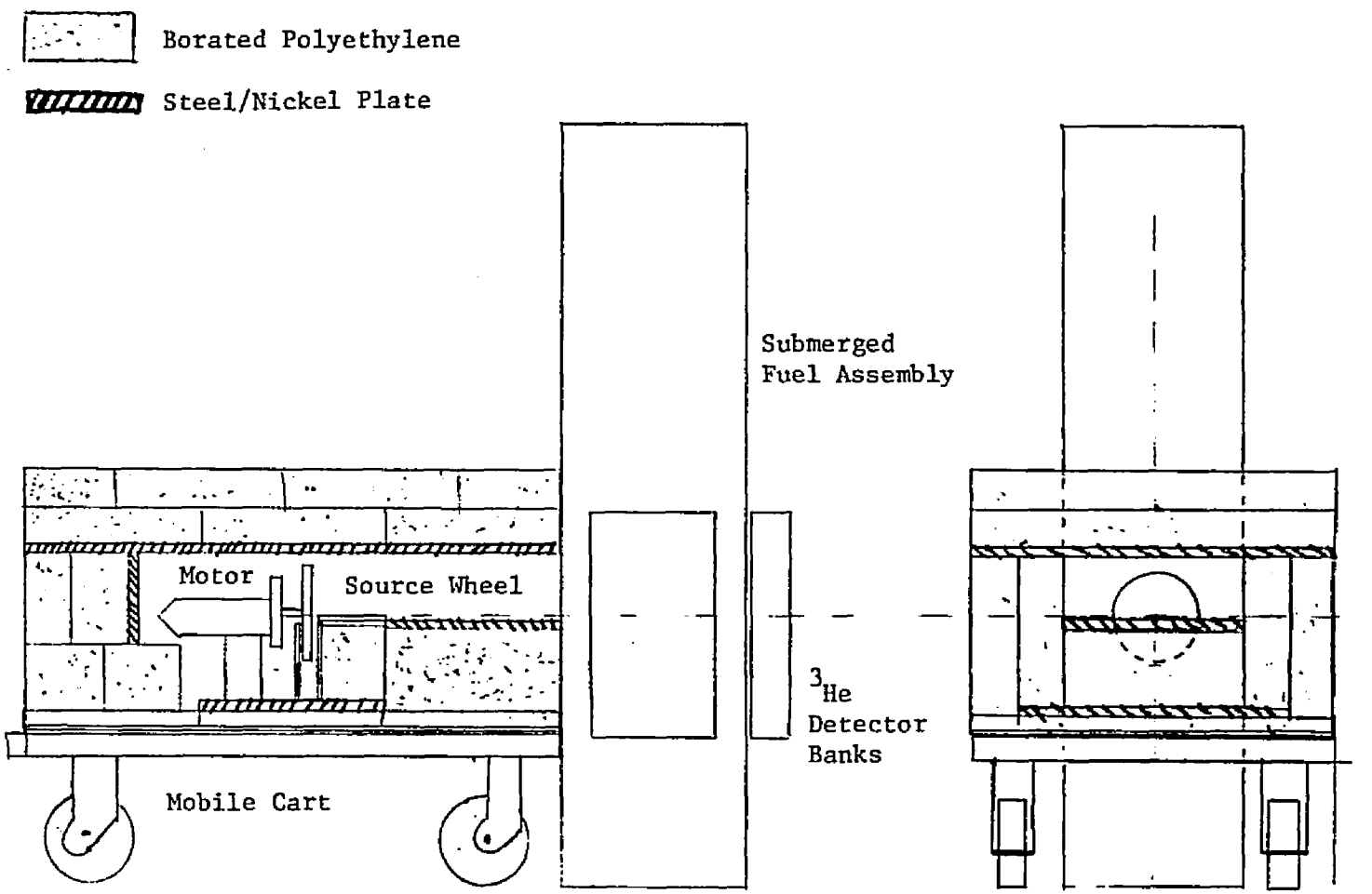

Figure A1. Spinning source neutron chopper.

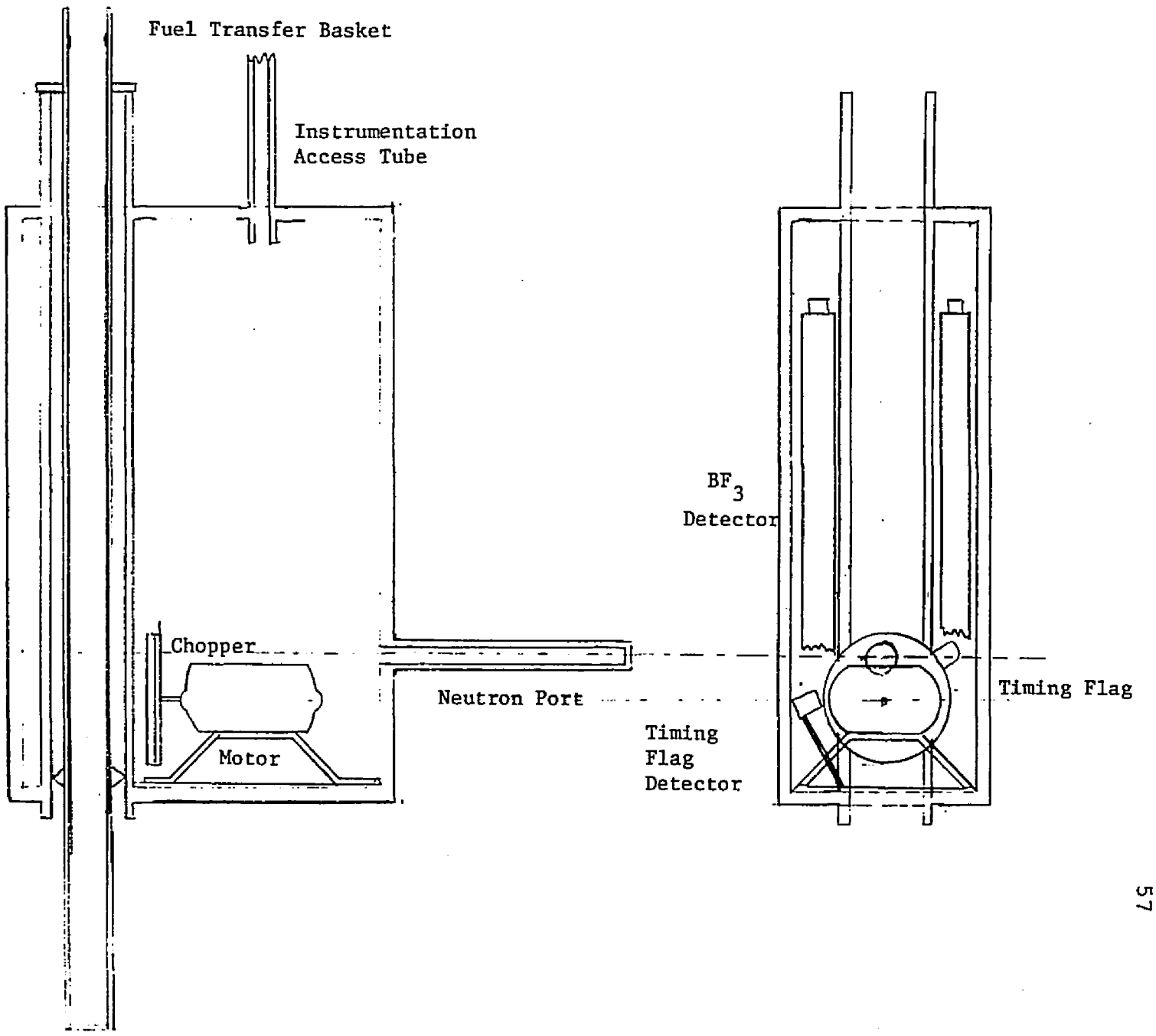

Figure A2. Constant source neutron chopper.

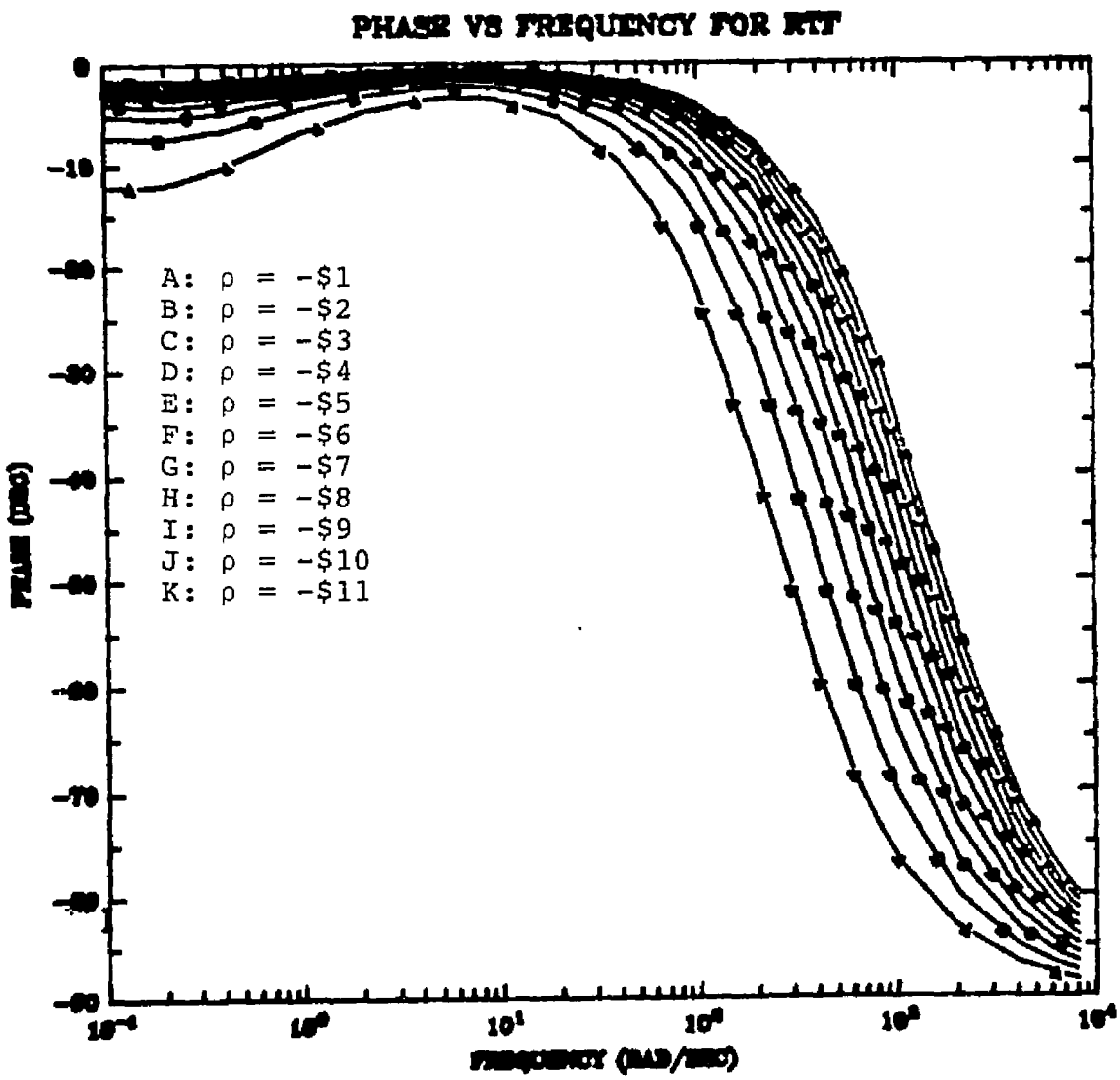

Figure A3. Phase of reactor transfer function versus frequency for various degrees of subcriticality.

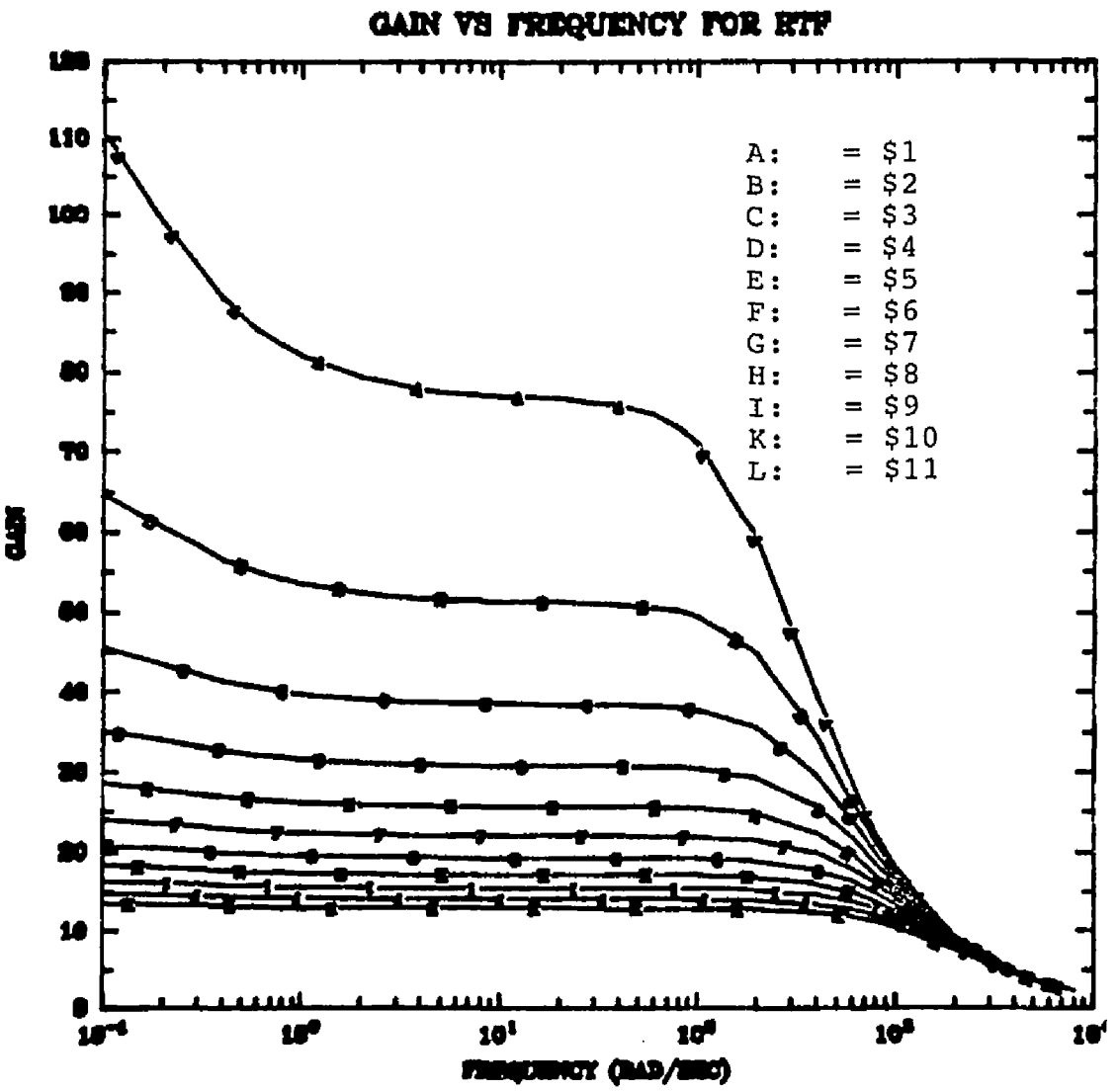

Figure A4. Gain of reactor transfer function versus frequency for various degrees of subcriticality.

corresponding to 10000 rev/min are necessary. The mechanical problems associated with rotating a reasonable massive source or shield block at an acceptable radius at these speeds are quite evident.

The system described in Figure A1 utilizes the spinning source. Feasibility testing of the spinning source chopper was conducted in mid 1983 at Los Alamos National Laboratory. The source was a 9 mCi Cf-252 sample enclosed in a stainless can. The assembly being interrogated was a fresh 15X15 PWR fuel assembly, 3.2% enriched in the U-235. Measurement of the effective multiplication factor produced a value of 0.9. Predictions of phase shift from the analytical expression in equation 2.2.19 yielded a value of 5 for a rotation rate of 870 rpm. Figures A5 and A6 show the raw data obtained. By numerical estimation, the phase was determined to be 4.5°. Although slightly higher frequencies were possible with this system, time constraints prevented further investigation.

The constant source chopper was applied to extremely subcritical samples. The source was the leakage flux from a TRIGA Reactor operating at a steady state of power level of 5 watts. The test assemblies were standard TRIGA fuel elements, in varying degrees of burnup. Although much higher effective frequencies were obtainable, 50000 rev/min, because of self-shielding and discrimination

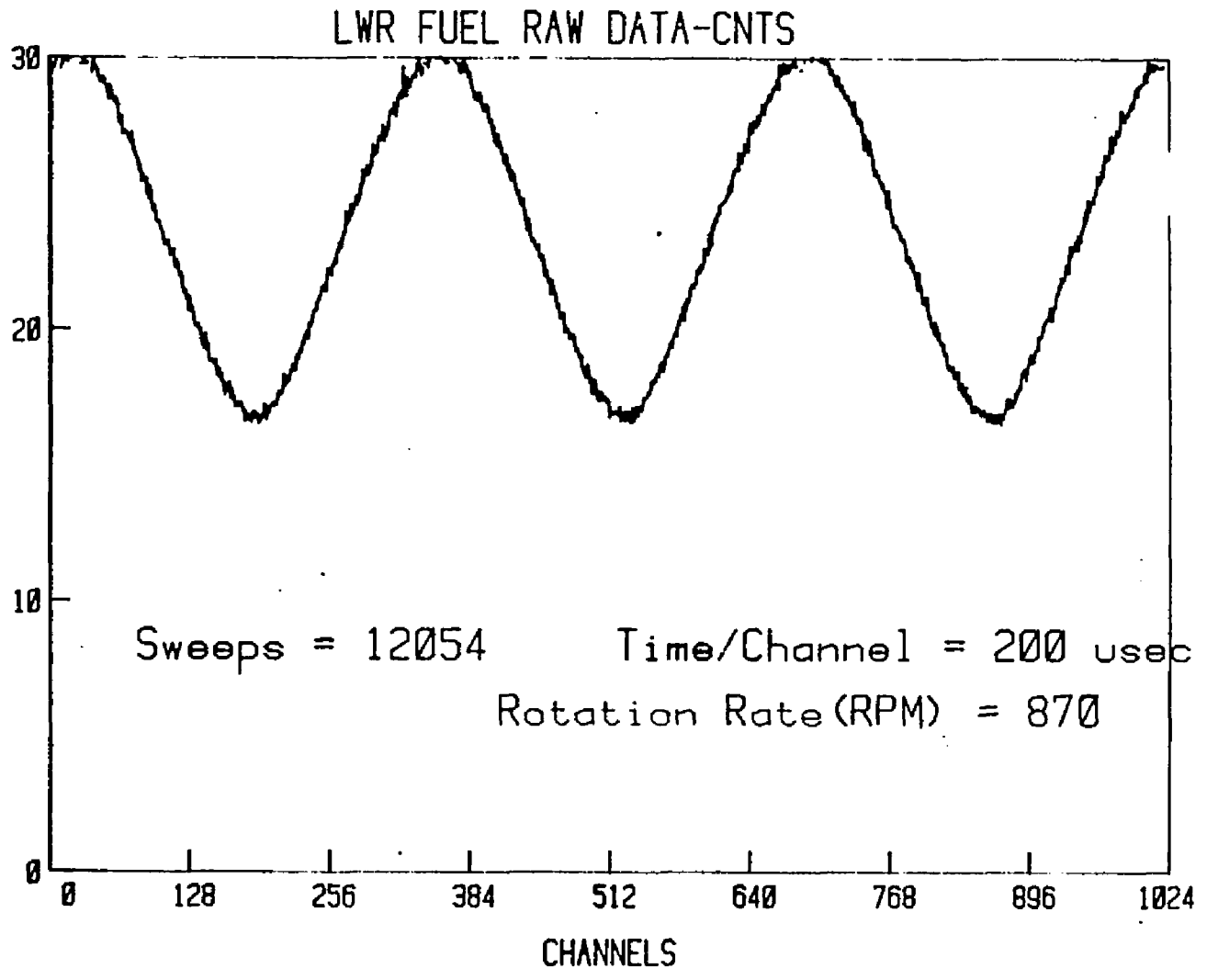

Figure A5. LWR fuel, raw data counts.

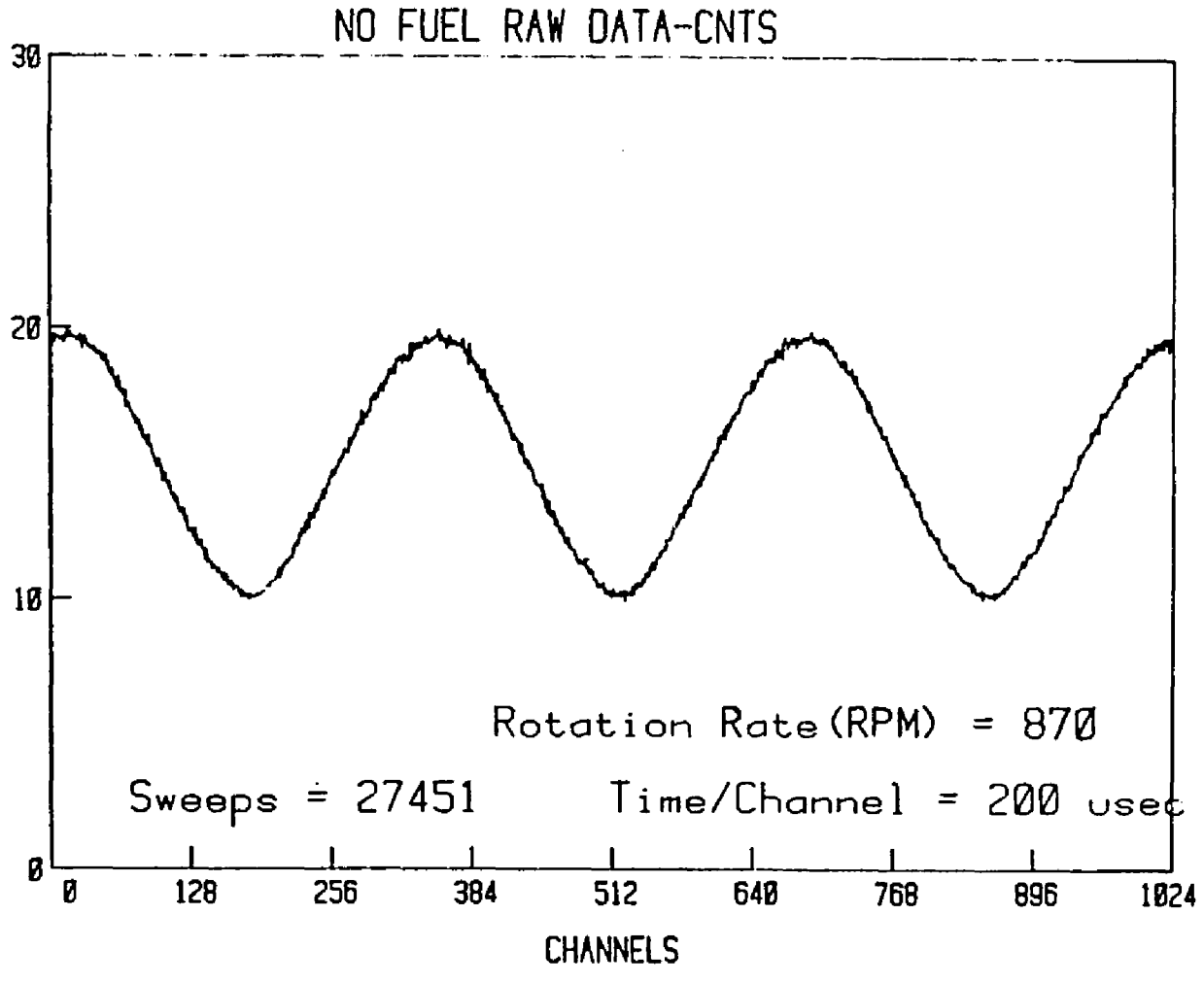

Figure A6. No fuel, raw data counts.

problems, no useful data could be collected. The discrimination problems were in distinguishing between the source neutrons and the fission neutrons from the sample. The theoretical signal-to-noise ratio (SNR) for reactivities $-100 at 50000 rev/min are 0.01. However, due to extremely small efficiencies in the detection system further compounded the already small SNR, the result was unusable data.

REFERENCES

Giozani, Tsahi. Active Non-Destructive Assay of Nuclear Material. Nuclear Regulatory Commission, 1981.

Lamarsa, John R. Introduction to Nuclear Reactor Theory. Addison Wesley Publishing Company, 1965.

Thie, J. A. Power Reactor Noise. American Nuclear Society, 1981.